UNIVERSITEIT VAN PRETORIA
UNIVERSITY OF PRETORIA
YUNIBESITHI YA PRETORIA

STRAIN MEASUREMENT VIA THE INNER SURFACE OF A ROLLING LARGE LUG TYRE

by

Megan Savannah Pegram

Submitted in partial fulfillment of the requirements for the degree
Master of Engineering (Mechanical Engineering)

in the

Department of Mechanical and Aeronautical Engineering
Faculty of Engineering, Built Environment and Information Technology

UNIVERSITY OF PRETORIA

October 2020

Abstract

The complex interface between tyre and terrain is a largely studied topic in terramechanics and vehicle dynamics research. This interface, known as the contact patch, is however hidden from view and cannot easily be measured. Several studies have focused on measuring tyre strain on the inside surface of the tyre to indirectly determine tyre parameters. The inner surface is separated from the contact patch by the tyre thickness however this difference can be considered small in comparison to the benefit gained by a safe environment for measurement systems. Static studies of tyre strain have been successful however lacks the important phenomena occurring in a rolling tyre. Tyre strain measurements in dynamic tyres have been limited to discrete points and/or once per revolution, which is an insufficient sampling rate for vehicle stability controllers such as ABS.

This study performs full-field and point strain measurements of the inner tyre surface of a rolling agricultural tyre at low speeds. Stereo cameras mounted on a mechanically stabilised rim will record full-field measurement of the contact patch kept in constant view. Digital Image Correlation techniques are used to determine full-field deformation and strain from successively captured images. Point measurements, such as strain gauges, are included in the study for a comparative measurement.

An agricultural tyre hosts large lugs which include large strain concentrations within the contact patch. The complex tyre structure significantly influences the strain measurements, other factors such as inflation pressure, vertical load and slip angle is also studied. Since most vehicle forces are transmitted through the tyre at the tyre-terrain interface, capabilities to measure this area will be a great benefit for tyre research and leading towards a smart tyre.

Acknowledgements

I would like to express my gratitude to:

- My mother, for her continuous love and support
- My supervisor, Dr Theunis Botha, who guided me throughout my post-graduate degree which not have been possible without his extensive knowledge on the topic
- Professor Schalk Els, for his insight and support as well as the opportunity to further my studies at VDG
- Glenn, Wietsche, Carl, Peet, Edwin and Tiano for their assistance during my prolonged setup and testing
- Monique, Wian, Andries and Wilhelm for their advice, support and everyday conversations
- Pascal, Jono and Blayne for their support and encouragement

List of Abbreviations

ABS	Anti-Lock Braking System
ADC	Analogue-to-Digital Converter
CAD	Computer Aided Design
CST	Constant Strain Triangle
DAQ	Data Aquisition
DIC	Digital Image Correlation
ESC	Electronic Stability Control
FEM	Finite Element Method
FPS	Frames Per Second
FRTM	Flexible Ring Tyre Model
LED	Light Emitting Diode
LI	Load Index
PSD	Position Sensitive Detector
SAW	Surface Acoustic Wave
T2Cam	Tyre Terrain Camera
TPMS	Tyre Pressure Monitoring System
ULP	Universal Low-Profile
UTC	Coordinated Universal Time
WFT	Wheel Force Transducer
3D	Three Dimensional

Nomenclature

Greek Symbols

α	Slip angle	$^\circ$
ϵ	Strain	
γ	Shear	
ν	Poisson's ratio	

Other Symbols

A	Area
r	Radius

Subscripts

x	Longitudinal
y	Lateral

Contents

1 Introduction **1**

2 Literature Study **3**
2.1 The Tyre . . . 3
2.2 Contact patch measurement:
Strain, deformation or acceleration testing . . . 4
2.2.1 Accelerometers . . . 4
2.2.2 Surface Acoustic Methods . . . 4
2.2.3 Piezoelectric sensors . . . 5
2.2.4 Capacitive sensors . . . 5
2.2.5 Strain gauges . . . 6
2.2.6 Optical sensor . . . 8
2.3 Studies performed on agricultural tyres . . . 9
2.4 Tyre testing . . . 11
2.4.1 Conclusion . . . 12

3 Strain measurement from digital images **14**
3.1 Tyre Terrain Camera (T2Cam) . . . 14
3.1.1 Power supply . . . 16
3.1.2 Triggering . . . 16
3.2 Camera Settings . . . 17
3.2.1 Lens Settings . . . 17
3.2.2 Camera Settings . . . 18
3.3 3D Measurement using Digital Image Correlation . . . 19
3.3.1 Strain algorithm . . . 20
3.3.2 Calibration . . . 21
3.3.3 Algorithm settings . . . 21

4 Full-field strain comparison between a passenger car tyre and an agricultural tyre **24**
4.1 Inner surface strain of smooth treaded tyre under static loads . . . 25
4.2 Inner surface strain of an agricultural tyre under static loads . . . 27
4.3 Conclusion . . . 28

5 Point strain measurement via the inside tyre surface **29**
5.1 Strain gauge location . . . 29
5.1.1 Static agricultural tyre . . . 29
5.2 Strain gauge wiring configurations . . . 32
5.3 Installed strain gauges . . . 34

6 Experimental Work and Results **35**
6.1 Artificially strained images . . . 35
6.2 Test Setup . . . 36
6.2.1 Strain gauges . . . 36
6.2.2 Drum roller . . . 37
6.2.3 Data capture . . . 38
6.3 Data post-processing . . . 39
6.3.1 Syncing Data . . . 39
6.3.2 Comparing strain gauges and T2Cam measurement . . . 41
6.3.3 Degrees to mm . . . 43
6.3.4 Dirt on lenses . . . 43
6.4 Comparison of static tests on a flat and drum test surface . . . 44
6.5 Strain gauge trends . . . 45
6.5.1 Vertical Loading . . . 46
6.5.2 Varied Slip angle . . . 49
6.5.3 Discussion of strain gauge results . . . 52
6.6 Differences in full-field to point measurements . . . 52
6.7 Effect of lug contact pattern . . . 54
6.8 T2Cam load sensitivity . . . 56
6.9 Comparison of different slip angles . . . 59
6.10 Discussion of results . . . 61

7 Conclusion and Discussion **63**

8 Recommendations **65**

List of Figures

2.1 Symmetrical longitudinal and lateral strain gauge trends for straight-line driving from literature (Morinaga et al., 2006) . . . 7
2.2 Strain gauge layout on the inner tyre surface, used by Garcia-Pozuelo et al. (2017a) . . . 8
2.3 Position of pressure sensors placed about the lugs of the tyre (a) (Raper et al., 1995) (b) (Jun et al., 2004) . . . 10
2.4 Effect of test surface curvature on contact patch deformation (Tuononen, 2011) 12

3.1 Schematic of Tyre-terrain camera (T2Cam) . . . 14
3.2 Improved T2Cam system fully assembled before being installed inside of the tyre . . . 16
3.3 Aperture f-stops . . . 18
3.4 The effect of gain on image captured of the inner surface contact patch . . . 19
3.5 Reference and Current images required for DIC algorithm . . . 20
3.6 Produced 3D Contact patch (Side view, Top view, Isometric view) . . . 20
3.7 Constant Strain Triangle (CST) used for in-plane strain measurement . . . 21
3.8 The effect of subset size on an image captured of the inner surface contact patch . . . 22
3.9 The effect of subset spacing on an image captured of the inner surface contact patch . . . 23

4.1 Smooth treaded and large lug tyre used for comparing the effect of tyre structure 24
4.2 STTR in longitudinal and vertical loading position with smooth treaded tyre installed . . . 25
4.3 Discrete longitudinal and lateral strain of a vertical loading test on smooth treaded tyre (3 Bar) . . . 25
4.4 Discrete longitudinal and lateral strain measurement along the centreline from a vertical loading test on smooth treaded tyre (3 Bar) . . . 26
4.5 Discrete longitudinal and lateral strain vertical loading test on agricultural tyre (2 Bar) . . . 27
4.6 Discrete longitudinal and lateral strain measurement along centreline for vertical loading test on agricultural tyre (2 Bar) . . . 28

5.1 Discrete longitudinal and lateral strain with increase in inflation pressure on an agricultural tyre . . . 30
5.2 Discrete longitudinal and lateral strain with increase in vertical load on an agricultural tyre (2 Bar) . . . 30

5.3 Point location for placement of strain gauges on inner surface of an agricultural tyre . . . 31
5.4 Inflation test, Vertical Test, Longitudinal Test (forward), Longitudinal Test (backward) and Lateral test on an agricultural tyre (2.0 Bar) . . . 32
5.5 (a) Quarter and (b) Half bridge configuration . . . 33
5.6 Micro-Measurements EP-08-125TM-350 strain gauge . . . 33
5.7 Installed inner surface strain gauges . . . 34

6.1 Speckle pattern used to test accuracy of strain measurements . . . 35
6.2 Surface after horizontal strain . . . 36
6.3 Surface after horizontal and vertical strain . . . 36
6.4 Dynamic test setup with agricultural tyre installed . . . 37
6.5 Trigger sequence used during testing . . . 39
6.6 Images captured during testing . . . 40
6.7 Inner surface strain gauges where silicon and lead wires can be seen to obscure the view of the installed region . . . 42
6.8 Method used to tracking a point from Frame 1 to Frame 2 . . . 42
6.9 Tracking method used to track a point (red) from Frame 1 to Frame 4 as it moves from the right to the left of the contact patch . . . 42
6.10 Method used to convert between millimetres to degrees . . . 43
6.11 Dirt on upwards facing lens . . . 44
6.12 Contact patch footprint of agricultural tyre vertically loaded onto a (a) Flat bed and (b) Drum . . . 45
6.13 Layout and configurations of strain gauges placed within the contact patch of agricultural tyre . . . 45
6.14 Longitudinal strain gauge results with increase in vertical load (2.0 Bar, 5km/h) with the results given as (a) Full Distribution (b) Zoomed in section . . . 46
6.15 Lateral strain gauge results with increase in vertical load with (a) all loads and (b), (c) are the results split up between low loads and high loads . . . 47
6.16 Key points for measurement for the inner surface strain distribution in the (A) longitudinal direction and the lateral direction at (B) low loads and (C) larger loads . . . 48
6.17 Maximum (a) Longitudinal and (b) Lateral tension and compression peak strains during vertical loading at 2.0 Bar . . . 48
6.18 (a) Longitudinal and (b) Lateral results at a low and high load at test pressures of 1.2, 1.6 and 2.0 Bar . . . 49
6.19 (a) Longitudinal and (b) Lateral strain distribution for varied slip angles at a vertical load $\approx$ 1600N . . . 49
6.20 Maximum (a) Longitudinal and (b) Lateral tension and compression peak strain measurements at different slip angles ($\approx$ 1600N) . . . 50
6.21 (a) Longitudinal and (b) Lateral strain distribution for varied slip angles at a vertical load $\approx$ 1300N . . . 50
6.22 (a) Longitudinal and (b) Lateral strain distribution for varied slip angles at a vertical load $\approx$ 700N . . . 51

6.23 Maximum lateral tension and compression peak strains at different slip angles at vertical loads of (a) ≈ 700N (b) ≈ 1300N 51
6.24 Compression peak values for lateral strain distribution at varied slip angles and vertical loads 52
6.25 Comparison of (a) Longitudinal and (b) Lateral strain from full-field and point measurement at three vertical loads (2.0 bar, 5km/h) 53
6.26 Changing contact between road and agricultural tyre 54
6.27 Longitudinal strain of discrete moments as tread block travels through contact patch 55
6.28 Lateral strain of discrete moments as tread block travels through contact patch 55
6.29 Waterfall plot of longitudinal strain showing movement of tread block through contact patch 56
6.30 Load sensitivity: Longitudinal and lateral strain along the centreline with increase in vertical load 57
6.31 Maximum (a) Longitudinal and (b) Lateral tension and compression peak strains with increase in vertical load (2.0 Bar, 5km/h) 58
6.32 Load sensitivity: Longitudinal and lateral strain along the centreline with increase in load (second region) 58
6.33 Maximum (a) Longitudinal and (b) Lateral tension and compression peak strains with increase in vertical load (2.0 Bar, 5km/h) 59
6.34 Slip angle sensitivity: Longitudinal and lateral strain along three lateral positions with change in slip angle (1600N, 2.0 Bar, 5km/h) 60
6.35 Maximum Longitudinal and Lateral tension and compression peak strains with change in slip angle (1600N, 2.0 Bar, 5km/h) 61

List of Tables

3.1 Camera and lens specifications 17

Chapter 1

Introduction

Aside from aerodynamic forces, all forces and moments acting on the vehicle occur through the tyre. The tyre, being the only interface between the vehicle and the road, has thus been the subject of many research studies. The area of contact between the tyre and road, otherwise known as the contact patch, is vastly studied to determine tyre excitation forces as well as tyre characteristics such as friction coefficient, slip ratio, road condition and tyre wear. Knowledge of the tyre forces and characteristics can be used to improve current vehicle stability systems by providing accurate vehicle state estimation. Tyre forces can and has been measured through the wheel hub with a Wheel Force Transducer (WFT) which is expensive, complex and not viable for commercial applications. Estimating the tyre forces directly from the tyre-road interface should lead to accurate and reliable results. Measuring from the outside tyre surface is, however, complex by the fact that the tyre tread wears away. Measurements such as acceleration and strain have been taken from the inside tyre surface as this allows for the measurement system to be fully protected inside the tyre regardless of the testing environment. The inside tyre surface is slightly removed from the outside surface by the tread, it has been shown that inner surface measurement can be used to provide valuable information of the phenomena occurring at the outer tyre surface.

Smart tyres have become a popular topic in tyre research where the tyre is no longer a passive element but rather a sensor in itself. Smart tyre studies aim to measure tyre characteristics and forces from either acceleration, strain or deflection measurements. Previous research has shown that inner surface strain is sensitive to changes in tyre driving conditions. The relationship between the driving conditions and strain is complex. These relationships can be obtained via experiments in the hope that they may lead to tyre states being estimated from strain measurement only. Strain measurement is commonly done, but not limited to, strategically placed discrete point measurement such as strain gauges and recently has been done using cameras for full-field measurement. Strain gauges offer an inexpensive sensor which is small, compatible and does not change nor negatively affect tyre properties. These point measurements only provide contact patch measurements once per revolution, including more sensors along the circumference will otherwise increase this. Additional to smart tyres, tyre measurement can be used for tyre model validation. Being able to measure inner surface deformation and strain will allow for better parametrisation of complex physics based models or finite element models. Sensors which can measure inner surface strain on deformable terrain is invaluable for tyre model validations where they are

often validated on surfaces not similar to typical road conditions.

Most studies are performed on passenger tyres where the tread is rather small, with very little studies done on agricultural tyres. Agricultural tyres have large lugs therefore the contact patch and inner tyre surface is further separated. The larger load path can cause interesting phenomena. Point sensors can be placed along the lugs in order to get measurements as close to the outer surface as possible, without damaging the sensors.

In this study, cameras paired with Digital Image Correlation (DIC) techniques are used to measure full-field inner surface strain in addition to point measurements using strain gauges on the inside. Both full-field and point measurements have their shortcomings where a compromise study is needed between accuracy and real-time capabilities. Both full-field and point strain measurements will provide valuable information in a rolling tyre. The work done in this study aims to measure strain in a rolling agricultural tyre in order to determine what the effect of changing tyre conditions are on the strain measurement. The order of this study is given below:

Chapter 2: The advances in smart tyre development is discussed. Strain, acceleration and deflection based smart tyres are explored and their suitability for in-tyre sensing.

Chapter 3: The full-field measurement system to be used in this study is introduced and explained. The Digital Image Correlation techniques are presented as well.

Chapter 4: The full-field measurement system was tested on two different tyres in a static nature. This was used to show key differences of the strain distribution in tyres of different structures.

Chapter 5: The results from Chapter 4 are used to identify point locations for strain gauges to be placed on the inner surface of an agricultural tyre.

Chapter 6: The full-field and point measurement systems are installed on an agricultural tyre and dynamically tested on a drum, the results and discussion for this is presented.

Chapter 2

Literature Study

2.1 The Tyre

The tyre serves the purpose of interfacing between the road and vehicle to transmit forces between the two whether the tyre is static or rolling. This important interface is, however, hidden from view and cannot be directly viewed except with the use of a glass surface. Having an extensive and in-depth understanding of this interface will lead to a better understanding of how the vehicle turns, brakes and accelerates. Current measurement systems such as Tyre Pressure Monitoring System (TPMS), enables tyre pressure to be constantly monitored to detect over- or under-inflation. Active safety systems, such as ABS, will greatly benefit from accurate and fast estimation of the tyre-road interface parameters (e.g. tyre-road friction coefficient) (Muller et al., 2003). Having the tyre become an active element in vehicle control could increase the accuracy of vehicle safety systems.

The tyre structure is complex with several layers of materials of different stiffness's. Rubber experiences large deformation while the reinforcing steel cords resists most of the tension and compression, therefore, experiencing little strain. The working conditions of the tyre is dependent on many factors such as driving surface, tyre pressure, tyre temperature etc. The tyre is a pneumatically pre-stressed doubly-curved surface, therefore, for a tyre to travel along a flat surface, the tyre will need to be stretched, compressed and bent. The more vertical load on the tyre, the more the tread ring is straightened in the contact patch from bending deformation. Predicting tyre behaviour is a highly non-linear process and requires advanced tyre models followed by a large amount of testing under several conditions.

Many methods have aimed to measure tyre parameters indirectly from either acceleration, strain, or deflection. Some of these methods are limited to indoor test rigs where the test surface is far from realistic road conditions. Tyre characteristics are greatly dependent on the road surface in terms of the mechanism of friction generation. A system which has testing capabilities on all road surfaces and conditions, including rain and dirt, is needed to turn the tyre into an active element.

The requirement for constant tyre monitoring becomes highly important for vehicle safety. If advanced information of tyre-road conditions is known, such as force generation and adhesion parameters, the performance of vehicle safety systems can be improved.

2.2 Contact patch measurement: Strain, deformation or acceleration testing

Research on the development of a smart tyres has worked on estimating the state of the tyre with the majority of these studies focusing on discrete point measurements. The state of the art in smart tyre research is discussed.

2.2.1 Accelerometers

Acceleration-based intelligent tyres use tri-axial accelerometers in varied quantities and locations. Many studies, which make use of accelerometers, aim to indirectly measure longitudinal slip, slip angle, tyre forces and tyre-road friction coefficient. Accelerometers are favourable due to their robustness, small size, cost, insensitivity to temperature and low power requirement. Accelerometers like many other sensors, need to be selected to endure the harsh conditions which they will undergo within the tyre.

Acceleration measurement, namely amplitude and distance between trailing and leading peaks, was seen to be influenced by changes in normal load, inflation pressure, road roughness, camber, slip angle and speed (Braghin et al., 2006). Niskanen and Tuononen (2014) found that the peak amplitudes were highly affected by high-frequency noise and that more information could be extracted by noting the distances between trailing and leading edges. Road interaction affects acceleration measurement with different noise levels present on different road surfaces. Niskanen and Tuononen (2014)'s accelerometer measurements gave noticeable contact length results on dry asphalt but became particularly noisy while on an aquaplaning pool. The tri-axial measurement is coupled with rotational, vibrational and gravitational accelerations therefore advanced post-processing techniques are required to extract useful data of the tyre-road interaction. Unlike some sensors, accelerometers are sensitive to rolling speed as this increases due to centripetal forces. Accelerations were seen to reach up to 400g's at a driving speed of 120km/h (Matilainen and Tuononen, 2015).

With a single accelerometer or several placed laterally, only one measurement per revolution is received which may not be suitable for vehicle control. Increasing the number of accelerometers throughout the circumference will increase the cost, energy requirement and processing complexity. A once per revolution update can be used to update the information sent to ABS in order to tune responses for the current road condition. A common placement of the accelerometers are three spread out laterally as done by Braghin et al. (2006); Niskanen and Tuononen (2014). Other placements are used to achieve different results such as slip angle measurement.

2.2.2 Surface Acoustic Methods

Pohl et al. (1999) aimed to estimate tyre-road friction coefficient by measuring the deformation of a single tread element. A Surface Acoustic Wave (SAW) sensor is completely passive and has a large frequency range which allowed for testing at high speeds. It also picked up fast deformation changes often seen when driving over wet surfaces. The deformation of the tread elements was measured using a pin inserted from the inside of the tyre into the tread

element which would act as a lever between two SAW elements. Each sensor was able to measure one in-plane strain direction. These sensors were not capable of measuring large deformations. Pohl et al. (1999) illustrated that the tyre-road friction coefficient could be estimated from deformation measurement of tread elements.

Kim et al. (2015) developed a SAW sensor for strain measurement of the inner surface of the tyre to be used to predict tyre forces and tyre-road friction. The sensor did not require a battery and made use of a self-energizing module. The study tested the effect of load and velocity on the strain experienced within the contact patch and found that the tension strain regions experienced increased strain with vertical load and decreased with increase in speed, while the compression strain regions remained rather unaffected. The study also found no correlation between the slip angle and the tyre strain, regardless of changes in the driving conditions. The study found that vertical load and longitudinal speed had the most noticeable effects on the tyre strains.

2.2.3 Piezoelectric sensors

With the presence of an electric field, physical deformation generates an electric charge in piezoelectric materials. Many studies use piezoelectric sensors with the aim of reducing the energy requirements for battery-powered sensors in the light of smart tyres. Piezoelectric films have shown the possibility of measuring strain over a wide portion of the tyre and not only at certain specific points (Lee et al., 2015). Piezoelectric sensors convert mechanical energy to electrical energy and thereafter used, in this case, for strain measurement. Different factors have effects on the energy harvesting of the sensor with one being rotational speed. Lee et al. (2015) found that the strains experienced in a static versus a quasi-static model where greater simply because the time period in which the sensor experienced the strain is different. Special considerations thus needs to be taken into account when testing with a piezoelectric sensor therefore, making the sensors distinctly dependent on rotational speed.

2.2.4 Capacitive sensors

With stiffness compatibility issues with many sensors, capacitive type sensors have utilised the reinforcing steel wires within the tyre as the sensing element (Matsuzaki et al., 2005). Making use of the steel wires will allow for measurement without disrupting the stress profile or tyre deformation. When the tread is deformed, the steel wires acting as the electrode are either compressed or tensed. The change in distance of the rubber dielectric between the two steel cords results in a change in capacitance for a single direction.

Matsuzaki and Todoroki (2007) developed an alternative sensor which enabled different locations, other than along the belt, to be measured. Matsuzaki and Todoroki (2007) aimed to provide an alternative to conventional high stiffness strain gauges with a flexible patch-type strain sensor with a wireless measurement system. A flexible strain sensor composed of two flexible substrates based on polyimide films within an ultra flexible epoxy resin is produced which measures strain from capacitance change. This sensor also has temperature compensation with the use of a dummy capacitor sensor.

Cao et al. (2016) developed a flexible bond wire capacitive strain sensor that has sufficiently low stiffness compared to the tyre rubber. The sensor was used for measuring the longitudinal strain on a vertically loaded static tyre. The sensor was positioned in the centre line of the tread via the inner surface of the tyre. This method was however not wireless and small fluctuations of measured capacitance were present during testing due to the possible movement of the wires. The sensor was able to measure strain accurately up to $\pm 6\%$ which is suitable for stiffer passenger tyres. The sensors did not give indications of the leading and trailing edge when tested statically by rotating the tyre and testing at several increments. Cao et al. (2016) believed that this was due to the test surface being on a drum and not a flat road.

Many of these studies were focused on producing a sensor suitable for mass production. A custom fabricated strain sensor can be useful when requiring a certain size and stiffness dependent on the test tyre.

2.2.5 Strain gauges

Strain gauges can measure tension and compression by the elongation and contraction of the applied surface by measuring the change in resistance across the gauge. Strain gauges can be wired in many configurations in order to eliminate or include certain measurements (e.g. temperature or bending moments). A big concern when making use of strain gauges is their application to the test surface. In order to achieve accurate results, the strain gauge needs to move with the test surface and not cause any local stiffening effects. An adhesive capable of transferring the strain from the test surface to the gauge and to return to its original state once unloaded is required. Having similar stiffness's between test surface and strain gauge is important, not only for prolonged use, but to achieve accurate and reliable measurements. With large deformations and/or prolonged use, there is a possibility of the strain gauge debonding from the test surface. Therefore, there are certain limitations with regard to testing and strain gauge locations. The reliability and durability of the gauges is certainly a prevalent issue. Garcia-Pozuelo et al. (2017a) was able to ensure the repeatability of strain gauges after repeatable results were seen after over 50 hours of testing.

Garcia-Pozuelo et al. (2019) found that strain measurements from strain gauges were not affected by the tyre's rotational speed and the noise level is lower than for accelerometers. The measured signal of the strain gauges are often very small, therefore, a Wheatstone bridge is almost always used. Strain gauges remain favourable due to their low cost and offer a feasible solution to measure strain under dynamic conditions, given the capability of a high sampling rate. When testing at low speeds ($<$20km/h), the velocity did not show notable effects, however, this should be tested at higher speeds with the expectation that the inertia effect will have a predominate effect on the strain.

The longitudinal and lateral strain via the inner surface of steady state straight line rolling tyre, as adapted from Morinaga et al. (2006), is seen in Figure 2.1. Strain in the two directions are seen to be fairly symmetrical at steady state conditions. The results shown in Figure 2.1 were a common trend of passenger car tyres. The symmetrical shape is due to the tyre deforming from a circular to a flat surface. A passenger tyre is relatively smooth

in comparison to agricultural tyres. A similar trend should be seen on an agricultural tyre due to this motion however the lugs will have an additional effect.

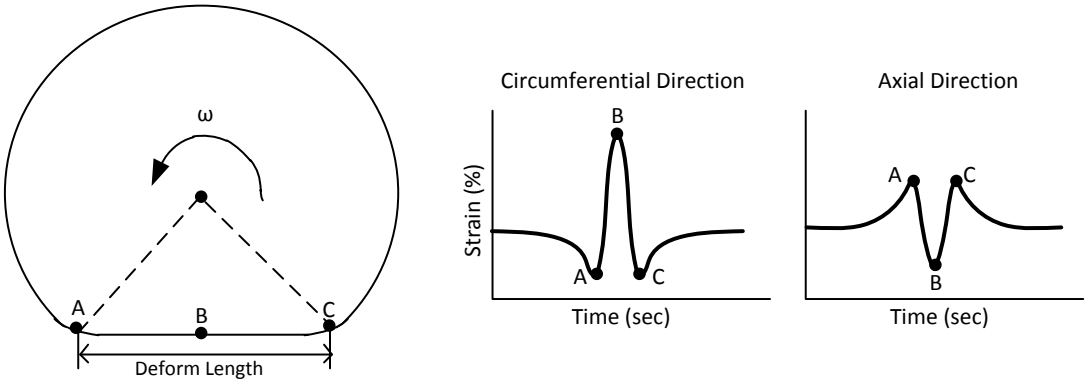

Figure 2.1: Symmetrical longitudinal and lateral strain gauge trends for straight-line driving from literature (Morinaga et al., 2006)

Yang (2011) used strain gauges to measure the lateral strain of the inner surface of the tyre. The lateral strain of a free rolling tyre at normal conditions had a symmetrical pattern. However, the pattern became asymmetric while under braking and traction ($\alpha = 0.05°$). The leading lateral tension peak (A in Figure 2.1) would increase and the trailing lateral tension peak (C in Figure 2.1) would decrease when under traction, and vice versa, for braking. This can be useful for predicting tyre conditions from strain peak values.

The longitudinal and lateral strain have converse relationships of each other which is expected based on the poisson ratio given in Equation 2.1.

$$\nu = -\frac{\epsilon_y}{\epsilon_x} \tag{2.1}$$

Large changes in strain are experienced as the tyre moves through the contact patch, regions of the tyre not in contact with the road are less affected. Changes in inflation pressure, speed and slip angle caused an increase in the offset value of the strain outside of the contact patch (Garcia-Pozuelo et al., 2017b).

The strain gauge layout used by Garcia-Pozuelo et al. (2019) (Figure 2.2) was successful in investigating slip angle changes, vertical load and speed on strain measurement within the contact patch. Quarter bridges were used with no temperature compensation. Without temperature compensation, the experimental results correlated well with a Flexible Ring Tyre Model (FRTM) used.

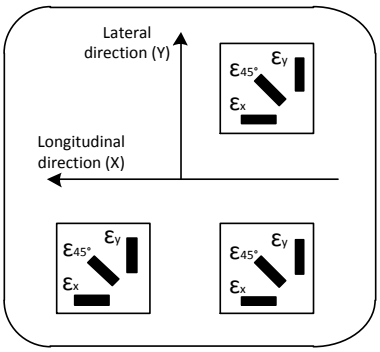

Figure 2.2: Strain gauge layout on the inner tyre surface, used by Garcia-Pozuelo et al. (2017a)

Strain gauges combine all effects into varying peak amplitudes and periods. The individual effects of tyre structure, rolling speed, pressure, normal load, camber angle, slip angle, slip ratio and wear will need to be taken into account. Studies using strain gauges have been, up to now, only conducted on passenger car tyres. The influences of the different parameters on passenger car tyres as seen in literature is given (Garcia-Pozuelo et al., 2017a, 2019):

- *Inflation pressure*: Increase in inflation pressure results in a stiffer tyre and thus strain peaks decrease with increase in inflation pressure.
- *Vertical Load*:
  - Longitudinal strain: Both the tension and compression peaks increased with increase in load however only the compression peak was seen to be linear
  - Lateral strain: The tension peaks increased linearly with increase in load. A third tension peak occurs between the two original tension peaks surpass a certain load and is due to increase in contact
- *Slip angle*: The loss of adhesion can be seen at higher slip angles on strain measurement. A close relationship between lateral force and maximum strain magnitudes was seen.
  - Longitudinal strain: Curve flattens with increase in slip angle
  - Lateral strain: The compression peak differs to zero slip and remains constant up to higher slip angles, when the tyre starts slipping, and then decreases.
- *Velocity*: Strain period will decrease with increase in speed. At speeds > 30km/h, the strain curve shifts downwards due to the increase in centrifugal force

2.2.6 Optical sensor

Tuononen (2008) developed an optical sensor to measure three-dimensional deflection of the inner tyre lining. The sensor made use of a Position Sensitive Detector (PSD) attached to the rim which detected the movement of a Light Emitting Diode (LED) which was embedded on the inner tyre lining. The LED however changed in intensity with change in angular displacement, therefore, readings were only meaningful at a few intervals per revolution. The relative position of the LED and PSD was also seen to easily change from

hard braking. The LED was installed through the rim and was found to imbalance the rim. The LED was later replaced by a laser (Tuononen, 2011). The laser's sampling rate only allowed deformation measurement up to 35m/s. Instead of measuring the direct distance of the LED, the Laser measures the radial distance to the inner surface.

Non-contact strain-based measurements are favourable to not alter test surface properties and to avoid debonding issues. A big advantage of cameras is their non-contact measurement. The use of cameras within the tyre application has been used both outside and inside the tyre. With many advantages of cameras, one being its whole field measuring capabilities. Secondly, a single camera image consists of a multitude of pixels of which each pixel can pose as a potential measurement point. Thus, numerous measurements can be obtained from a single image.

Hiraoka et al. (2009) proposed measuring out-of-plane deformation and in-plane strain of the inner tyre surface with a single camera and a laser, which created a speckle pattern. A single camera was mounted on the rim pointing at the inner tyre surface. The deformation measurement used to determine in-plane strain is calculated from the inner surface speckle pattern. The out-of-plane deformation uses the location of the laser, with the camera capturing its change in position, this change relative to its original position is then measured. The laser is used to remove the effects of radial displacement caused by out-of-place displacement to achieve accurate in-plane strain. This required two successive images, with and without the laser diodes, which is not possible on a normally rotating tyre. Hiraoka et al. (2009)'s results led the way for non-contact full-field measurement of the strain distribution of the inner tyre surface.

Green (2011) attempted to rectify the issues experienced by Hiraoka et al. (2009) regarding out-of-plane deformation when measuring full-field strain with a single camera. With a few limitations, Green (2011) was only able to improve the accuracy with a finer sub-pixel interpolation when locating points as compared to Hiraoka et al. (2009). The work done by Green (2011) took another step forward for non-contact full-field measurement. The study could not promise accurate results, however the trends were promising, with noticeable increase in strain with increase in vertical loading of the tyre.

The inner surface strain of a static agricultural tyre was studied by Feldesi et al. (2020), using two cameras inside of the tyre. A relationship was seen between change in tyre states (e.g. load and inflation pressure) and longitudinal and lateral strain measurements. The lug pattern had a significant effect on the strain patterns produced, while only tested in a static condition, this effect is expected for a rolling tyre. Full-field measurement thus becomes imperative for agricultural tyres, due to different regions of strain concentrations which would not be sufficiently measured with discrete point measurements. It must be noted that the test tyre in this current study is the same used by Feldesi et al. (2020).

2.3 Studies performed on agricultural tyres

An agricultural tyre has a complex geometry mainly due to its large tread blocks/lugs. These lugs are pure rubber or made up of a rubber-like material that experiences high de-

formations. Most tyre measurement studies are performed on passenger car tyres and few on agricultural tyres. The studies focusing on agricultural tyres are often based on reduction of inflation pressure to reduce the stress caused on the agricultural soil at high wheel loads. Additional to the work done by Feldesi et al. (2020), two additional studies are mentioned making use of agricultural tyres. Raper et al. (1995) instrumented an agricultural tyre with pressure transducers both on the lug of the tyre and in the under-tread. The layout is seen in Figure 2.3(a). Again, this study aimed at understanding the influence tyre pressure has on soil stresses. Four transducers were placed along the length of a single lug. It was found that the two closest lugs sensors to the tyre sidewall were most sensitive to tyre dynamic load while the two closest the centre of the tyre were most sensitive to inflation pressure. The under-tread transducers were influenced more by the dynamic load versus the inflation pressure. The large tread blocks of an agricultural tyre allow for many locations to insert sensors for contact patch studies.

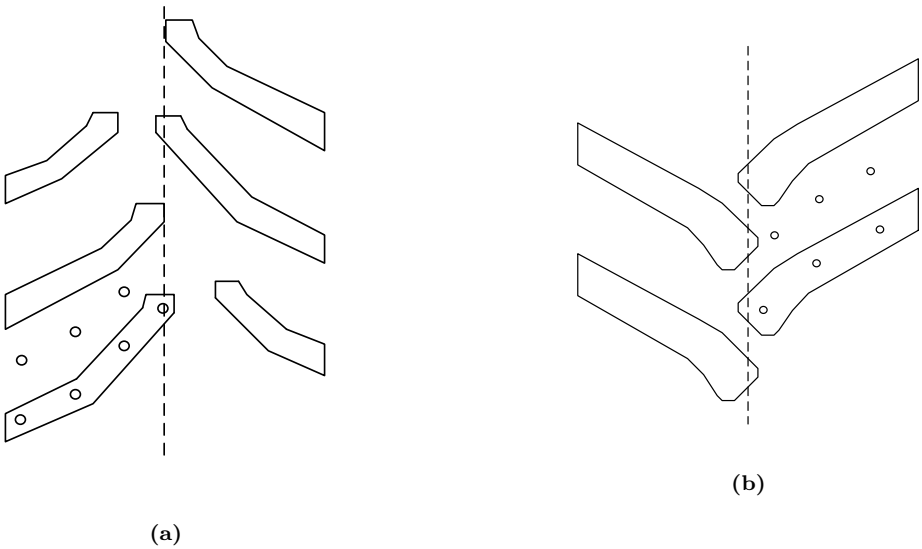

(a) **(b)**

Figure 2.3: Position of pressure sensors placed about the lugs of the tyre (a) (Raper et al., 1995) (b) (Jun et al., 2004)

Jun et al. (2004) conducted a study on the contact pressure measured on the lug and under-tread of a Trelleborg Twin tyre. With pressure transducers placed on the lug and under-tread measuring normal pressures. The layout is seen in Figure 2.3(b). The study tested at high load, low load, under-inflation and over-inflation. The four cases led to interesting results and differences between under-tread and lug contact pressures. It was found that the peak pressures on the lug were found towards the leading edge while the peak pressures on the under-tread appeared towards the trailing edge.

Agricultural tyre studies are focused around terrain stresses and the effects of different operating conditions via the outside surface. A study based on agricultural tyres inner surface strain is certainly a new development.

2.4 Tyre testing

Choice and development of sensors are important in order to measure key tyre characteristics. However, the type of tyre testing is also important to imitate normal driving conditions. Controlled environments are valuable in terms of repeatability and to allow comparison of results in order to find individual effects from specific changing factors.

Certain sensors are only suitable for static testing, therefore, limiting their capabilities of measuring real world driving conditions. Sensors should not change tyre properties nor extensively hinder it from normal driving conditions. Literature has shown many different static test rigs which inherently can provide highly controlled testing procedures.

Static testing includes pushing a test surface on a static tyre or vice versa. Test surfaces include flat beds and drums. Actuated static test rigs can be well-controlled and enables large load testing. Static test rigs reduce complexity and offer suitable options for testing of large tyres. Typical static test rigs can load a fixed tyre with an actuator in one to three of the loading conditions.

Cao et al. (2016) statically tested a strain sensor placed on the tyre inner surface centre line. The sensor was loaded onto a drum at incremental angles from the start to the end of the contact patch. The tyre did not experience compression before and after the contact patch as is experienced during typical straight-line rotation.

Glass panes have been used to view the contact patch through the other side of the glass (Ivanov, 2010; Castillo et al., 2006). Cameras beneath the surface can record the changes in the contact patch for full-field measurement. These rigs are often seen to have low speed capabilities. Being able to visually see the contact patch is incredibly valuable, however, glass plane studies lack the important tyre-road interaction adhesion mechanisms. Niskanen and Tuononen (2014) performed aquaplaning on glass, the smoothness of the glass was seen to have no realistic surface roughness and, therefore, should not be used for friction analysis. Testing dynamically on glass has a limited travel distance. Therefore, glass pane test rigs should be limited to static testing given the benefit of having the test surface become a viewing surface.

Tuononen (2011) dynamically tested deformation of the inner tyre surface at the same speed on different test surfaces. Figure 2.4 shows the difference in tyre deformation captured by the study. Tyre testing on a drum was found to experience larger deformations given the large r = 1.219m curvature.

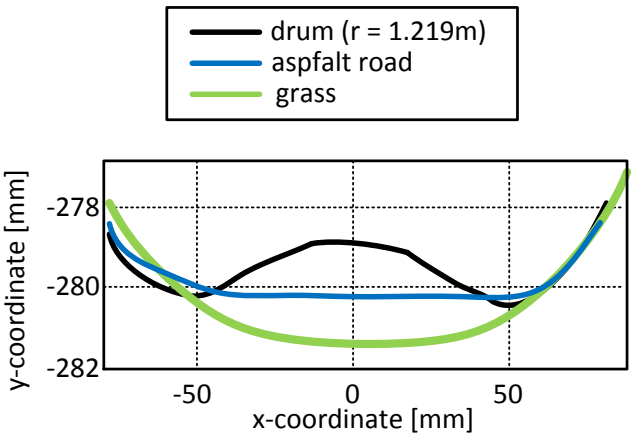

Figure 2.4: Effect of test surface curvature on contact patch deformation (Tuononen, 2011)

Other dynamic test beds which imitates the driving environment are flat dynamic tracks as used by Kim et al. (2015) and Erdogan et al. (2011). Many variables are changeable to perform straight-line and cornering tests. Flat tracks are favourable as they do not distort the shape of the contact patch or differ the operating conditions of tyres.

Many of the above test systems also allow for change of surface. With the glass surface rigs allowing inclusion of water for hydro-planing tests and other rigs can install rough sheets on the test surface for higher friction testing. An important add-on would also be the addition of traction or braking test capabilities.

Asides from measuring the contact patch with sensors attached to the tyre, studies have placed sensors on the flat test surface (Anghelache and Moisescu, 2011). Other tyre test rigs have included tyre shakers to test the tyre's non-linearity at high frequencies (Brusarosco et al., 2008).

Mimicking normal driving conditions is important to extract valuable data from tyre testing, choice of test rig paired with correct choice of sensor will give valued insight into how the tyre operates. Dynamic tests are much more valuable than static tests on a surface that is most representative of real road. A drum will be used for dynamic testing in this study, which is not ideal, however this is what was available to this study.

2.4.1 Conclusion

All the studies above have the same final objective of developing a smart tyre. The studies aim to measure tyre characteristics such as friction coefficient, forces, slip angle and slip ratio indirectly from the tyre inner surface from either strain, acceleration, or deflection measurements. Strain was typically measured with either strain gauges or cameras. Strain gauges show the possibility of measuring changes in tyre states with a point strain measurement, requiring little additional post-processing. Camera systems can measure full-field strain, equivalent to a multitude of strain gauges. Inner surface strain was seen to be sensitive to all changes in tyre states including load, inflation pressure, velocity and slip angle.

However, not all were a linear relationship. Both strain measurement sensors do not affect tyre properties and performances. Strain measurement of the inner tyre surface is thus a viable option for in-tyre sensing.

Most smart tyre research is performed on passenger tyres. Passenger tyres are relatively smooth in comparison to agricultural tyres and therefore will react differently. Little research has been done on agricultural tyres, with Feldesi et al. (2020) being the first to explore inner surface strain measurement of a static agricultural tyre. Feldesi et al. (2020) showed that strain measurement is highly dependent on tyre structure. Non-homogeneous strain patterns were experienced and strain concentrations occurred at locations where there were lugs. Full-field strain measurement has only been performed inside a static tyre and thus work still remains for a rolling tyre.

Many sensors are only suitable for static testing, but with the static and dynamic contact patch being different - there is a need for dynamic measurement. Sensors, which are capable of dynamic measurement, are often limited to one contact patch measurement per revolution which is not suitable especially when working towards being able to improve vehicle control system approximations. Little research exists where the contact patch is in constant measurement within a rolling tyre.

This study will perform both point and full-field inner surface strain measurement using strain gauges and cameras respectively. These two measurements will be done on an agricultural tyre during drum tests. Strain measurement is inherently different in a static tyre versus a rolling tyre, therefore the two sensors will be used for comparison purposes.

Chapter 3

Strain measurement from digital images

3.1 Tyre Terrain Camera (T2Cam)

A strain-based intelligent tyre prototype, developed by the Vehicle Dynamics Group at the University of Pretoria, provides a novel in-tyre measurement system for the inner tyre surface. The system developed by Guthrie et al. (2017) makes use of two stereo cameras and an on-board computer mounted on a stabilisation mechanism within the tyre. The stabilisation mechanism forms part of one half of a split rim. With the stabilisation mechanism, the cameras can be kept in focus of the contact patch in a static and a dynamic condition, and in fact in view of any chosen region within the tyre. A schematic of the installed system is given in Figure 3.1.

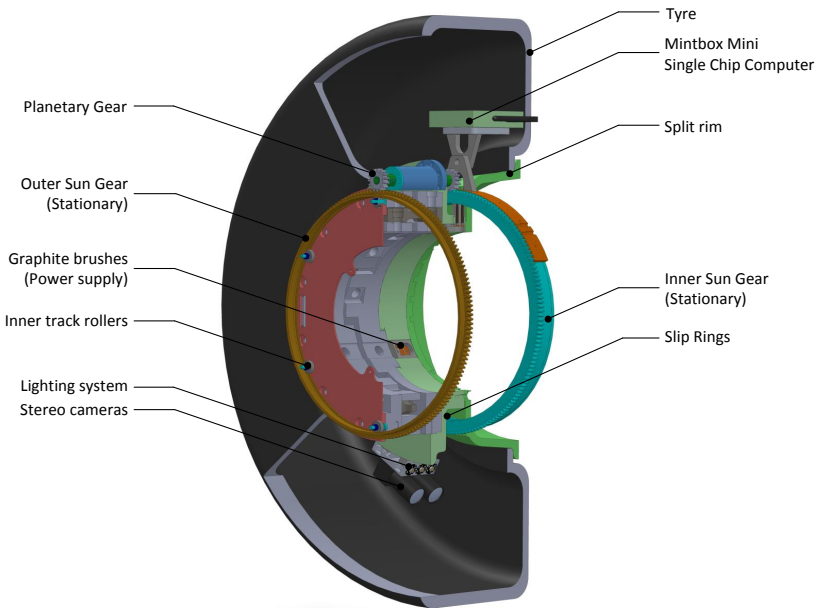

Figure 3.1: Schematic of Tyre-terrain camera (T2Cam)

The concept behind the stabilisation mechanism is a pair of planetary gears and sun gears; with one planetary-sun gear pair inside the tyre and one outside the tyre. The number of teeth of the two sun gears are equal as well as the two planetary gears. The two planetary gears are located on the same shaft and rotate with the tyre. The cameras and computer are mounted on the inner sun gear. Keeping the outer sun gear stationary will therefore, keep the inside sun gear stationary as well as keeping the cameras in the same position. The outer sun gear is kept stationary by a casing fixed to a stabilising torque arm, the full test setup will be discussed in Chapter 6.

From continuous images captured of the contact patch, image pairs can be compared to determine full-field deformation of the inner tyre surface. The first iteration of the system, as seen in Figure 3.1, positioned the two cameras side by side with minimal additional lighting. Both cameras facing the front of the contact patch from the trailing end, resulted in areas further away from the cameras having a decreased resolution and thus poor correlation of the full region. Side by side positioning has a limited baseline and thus inherently will not produce the best depth resolution. Even with the narrow baseline, Guthrie et al. (2017) was able to prove that inner surface tyre deformation could be measured dynamically. The developed concept provides a safe environment for the system to test regardless of the testing conditions and ensures that no dirt, or bumps, damages the system. This system has massive potential to measure many important parameters such as slip angle (Botha and Els, 2014), tyre velocity (Guthrie et al., 2015), rolling radius (Botha et al., 2015) and with advanced analysis tyre-road friction coefficient, however, only strain measurement will be focused on in this study.

The system is used at low rolling speeds, thus the added weight will not greatly affect inertial properties of the tyre. The system is non-contact thus will not affect local deformations of the tyre. With the system measuring strain from the inner surface as opposed to the outer surface, where the forces are applied, it is expected that the strain is attenuated because of the tread thickness in between the two layers. Understanding the relationship between inner and outer strain is non-trivial given the many different layers in between the two such as reinforcement layers and belt materials etc,.

Both the setup and the Digital Image Correlation (DIC) algorithm used had great potential and changes were suggested and then implemented by Feldesi et al. (2019) to further the capabilities of the system for strain measurement. Feldesi et al. (2019) improved the system by placing one camera on either side of the contact patch and included LED boards around the cameras lenses. The LED boards were used for strobe lighting which produced better illuminated images with less blur. The improved system is seen in Figure 3.2.

The amount of points tracked was drastically improved and allowed for more accurate measurements for larger strain applications. The original and improved camera setup were compared by capturing the same geometrically known surface. The point clouds of the surface from the two setups were computed with the same DIC algorithm and then compared to the Computer Aided Design (CAD) of the surface. The point to mesh distance found that the wide baseline improved the accuracy of the points measured by a factor of 3 compared to the narrow baseline. Providing additional lighting will allow for a shorter

required shutter time which is important in a rolling tyre to avoid motion blur. The LED rings added around both cameras provided even lighting around the contact patch without inducing glare. Strobing was used for the LEDs when capturing an image for a minimal power requirement. The LEDs and cameras shared the same trigger thus were triggered simultaneously.

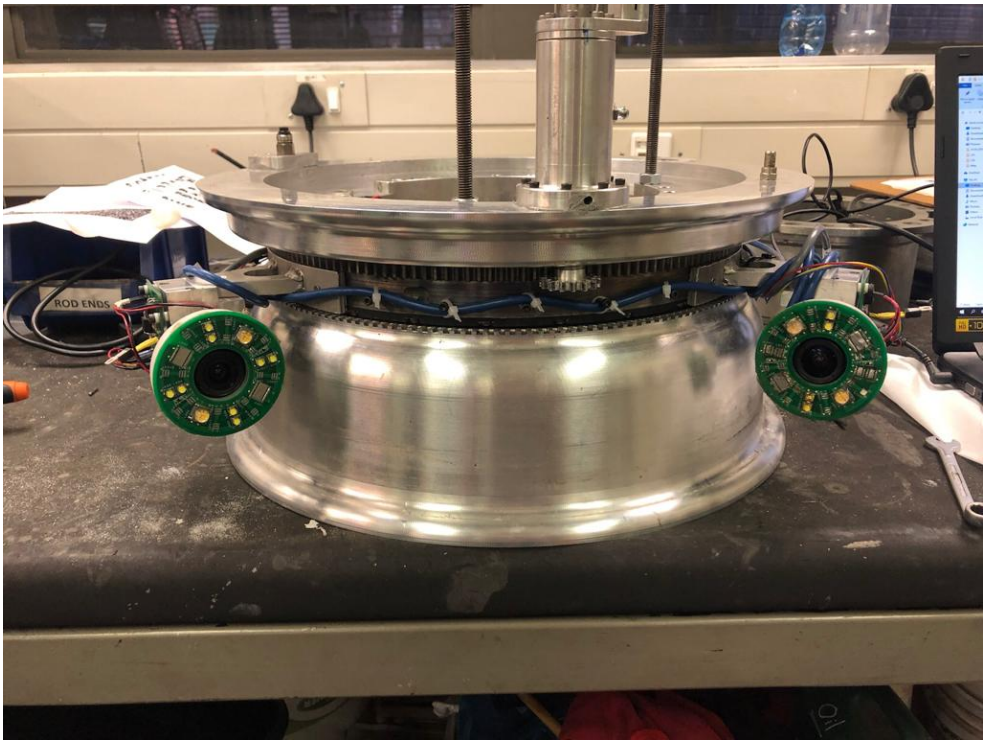

Figure 3.2: Improved T2Cam system fully assembled before being installed inside of the tyre

3.1.1 Power supply

A 12V power supply is required to power the cameras and computer. The power is fed through to the in-tyre system via three brush assemblies around the tyre circumference. The three points allow for continuous contact between brushes and slip ring and therefore no need for an on-board battery. The power supply as well as the cameras are stationary, two slip ring conversions are used between to provide power to the cameras. The first is through the telemetry and the second is within the tyre.

3.1.2 Triggering

On one side of the split rim, the surface has 172 teeth cut throughout the circumference. A relative encoder mounted on the second split rim facing these teeth are tuned to the trough of the teeth. The teeth are used to trigger the two cameras and LED's approximately every 2 degrees. The cameras are therefore only triggered when there is motion although during static testing, the cameras and LED's can be manually triggered.

There is no direct reference between images captured on the inside of the tyre and the absolute encoder measurement from the outside of the tyre. The data synchronisation taking this into account is discussed in detail in Chapter 6.3.

3.2 Camera Settings

Digital Image Correlation requires clear and well exposed images thus camera settings are crucial to successfully detect image points. Artificial lighting is used in the form of strobe lighting to provide sufficient lighting to the environment. The camera and lens settings are then tuned to give the needed exposure with no motion blur. T2Cam makes use of two cameras in order to extract three-dimensional information of the recorded images. The two cameras used in T2Cam are PointGrey FL3-U3-13Y3M-C cameras fitted with Kowa LM4NCL lenses, their specifications are given below in Table 3.1.

Specification	
Resolution	1280 ×1024
Frame rate	150 FPS
Sensor Type and Format	CMOS 1/2”
Shutter Type	Global
Lens Angle of View	103.6° vertical, 76.6° horizontal
Focal length	3.5 mm

Table 3.1: Camera and lens specifications

While the choice in cameras was an important decision and the success of the stereovision relied heavily theron, this however was not the focus of this study. An in detail focus on camera basic and cameras specific to this study is found in Guthrie et al. (2017); Botha (2015).

Without considerations given to motion blur, the maximum speed which T2Cam can be tested at is limited by the camera's frame rate of 150 FPS. The camera's are triggered every 2.09°/0.036 radians. The frame rate therefore allows a rotational speed of $5.47 rad/s$ which is just below $7 km/h$. This is, however, capturing an image for every trigger. Faster speeds can be achieved by capturing an image every second trigger.

3.2.1 Lens Settings

The fixed focal lens used requires aperture and focal length to be set. These settings are discussed and how they are tuned to be suitable for the environment inside the tyre below.

Aperture

The aperture size controls the amount of light entering through to the camera sensor. This is measured in logarithmically increasing f-stops where a lower number is a large aperture opening as shown in Figure 3.3. Having the aperture set fully open would allow in as much light as possible thus reducing the shutter time and additional lighting requirement. A

large aperture opening, however, reduces the depth of field and the distance between the furthest and closest in-focus object. With the focus area changes known, Feldesi et al. (2019) optimised this setting to have a depth of field of 0.2m and a suitable aperture for this was found to be 4.12.

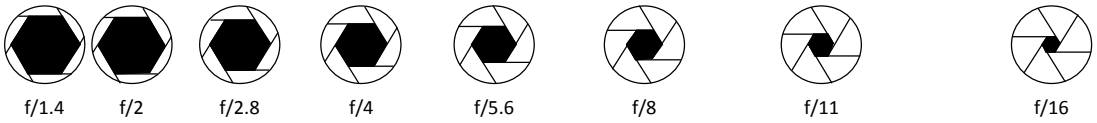

Figure 3.3: Aperture f-stops

Focal length

The lens has a fixed focal length of 3.5mm, however, adjusting the lens focus changes the focal length slightly. The focal length has no effect on the image exposure, however, requires a compromise on captured region and its magnification. The focal length describes the distance between the lens and the plane in which the light rays converge to form a clear image of the captured scene. Decreasing the focal length will increase the image range, however, this will be less magnified. The focal length thus has an effect on the camera calibration. This setting needs to be chosen with care as it cannot be changed once installed in the tyre. The focal length must be set to focus on the area of measurement. This was set to the centre of the contact patch.

3.2.2 Camera Settings

A digital image records each points luminance as a digital value ranging between 0 and 255. How the image sensor is exposed to light and converts this to a digital value, is determined by the two settings discussed below.

Shutter time

A variable setting, throughout testing, is the shutter time which is the time which the photo diode is exposed to light. This variable presents a compromise between limiting motion blur and having well exposed images. When the recorded environment does not have sufficient light, a longer shutter time is required, however, if there is movement while the shutter is open this could result in motion blur. Additional lighting is important inside the sealed tyre, with the LED rings as well as shutter time and aperture, these settings were used to capture well exposed images. The LED rings lighting could be increased to match the requirements in the tyre, increasing the lighting provided would allow for a shorter shutter time. The shutter time and strobe are both dependent such that a shorter shutter time will allow for a shorter strobe time and vice versa. An analysis by Feldesi et al. (2019) found a suitable shutter time to be 1ms.

Sensitivity/Gain/ISO

The gain is simply the amount that the analogue signal is amplified before the digitisation occurs at the Analogue-to-Digital Converter (ADC). A higher gain results in a more sensitive

sensor and a reduced additional lighting requirement. While the upper bound of this setting is favourable, it does however, bring about unwanted noise. A section of the tyre was captured with the gain varied while keeping the other setting constant as seen in Figure 3.4. A suitable gain was found by incrementally increasing the gain up to the point where the number of points detected decreased. A gain of 9 was used in this case as it was suitable for the compromise between sensitivity and noise. The process of achieving the point clouds below is discussed in detail in the next section.

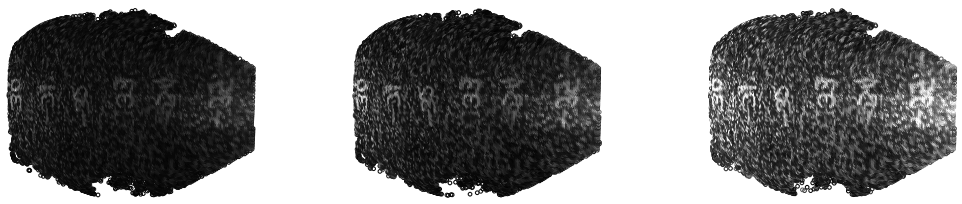

(a) Gain = 2 (No. of Points = 28018) **(b)** Gain = 9 (No. of Points = 28306) **(c)** Gain = 15 (No. of Points = 27792)

Figure 3.4: The effect of gain on image captured of the inner surface contact patch

The exposure of the image increases as the gain value increases with the effect of noise not very evident. The number of points captured does not vary greatly with change in gain. However, this does give some indication that neither too low or too high a gain is suitable.

3.3 3D Measurement using Digital Image Correlation

T2Cam comprises of two cameras which capture the inner tyre surface, with an image taken by the leading and trailing camera at the same instant. The two captured images are referred to as an image pair. Digital Image Correlation (DIC) techniques are used to attain three-dimensional (3D) measurement of the inner tyre surface from a 2D image pair. The two images belonging to an image pair is correlated using a subset window where common regions are identified by comparing the region's intensity levels. The window is allowed to deform between images to take into account different viewing angles and straining of the surface. Regions which correlate well are transformed into a 3D mapping using triangulation, the orientation and translation between the two cameras and the lens intrinsic parameters known from calibration, this process is presented by Botha and Els (2014).

The deformation from one time instance or state to the next is measured between the image pairs of the two states, namely a reference and current state. The reference state is the 'zero' deformation reference and the deformation measured is the deformation imposed on the surface between reference and current state. In this context, the reference state is usually set to the unloaded inflated tyre to isolate the sole effect of loading. In total four images are needed for a 3D deformation measurement as seen in Figure 3.5 where each image pair consists of two images from the two cameras of a single time instance.

The four images allow for the mapping of a 3D contact patch in two different states, from which the deformation will be obtained. The deformation is obtained by using a correlation algorithm on all images by tracking the location of a region not only between image pairs

but also different states. Thus, the deformation produced is the relative movement between the states. The images are processed into point clouds where each point is the 3D coordinate of the inner tyre surface in reference to the left camera's coordinate system.

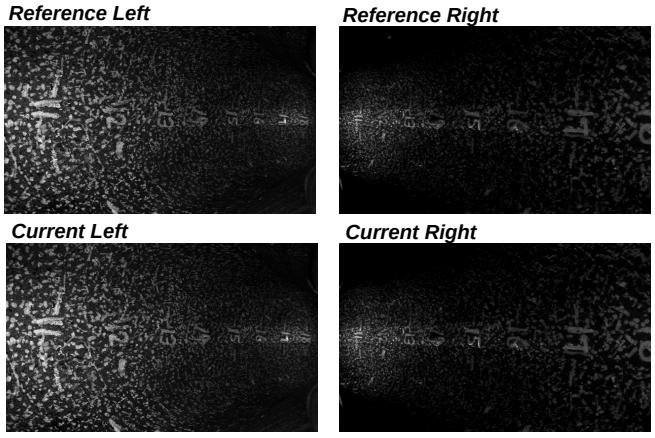

Figure 3.5: Reference and Current images required for DIC algorithm

The 3D point cloud for the reference state computed from the four images in Figure 3.5 is given in Figure 3.6. The 3D mapping of the inner surface contact patch can thus be produced. The top view of the contact patch will be used when presenting results in this study.

Figure 3.6: Produced 3D Contact patch (Side view, Top view, Isometric view)

3.3.1 Strain algorithm

DIC techniques produce a three-dimensional position and deformation field of the contact patch, this is used to calculate the contact patch strain field from the reference to current state. Strain is measured relative to the global axis system where x is along the longitudinal axis, y is perpendicular to x in the lateral axis and z is normal to the measured surface. The z direction is therefore constantly changing whilst the x and y axis remain constant.

Strain

Strain is the ratio of change in length to initial length. The three-dimensional position and deformation of the contact patch only allows for in-plane strain measurement, there-

fore, limiting the strain measurement to two-dimensional. The strain over the surface is calculated using a constant strain triangle (CST), as seen in Figure 3.7.

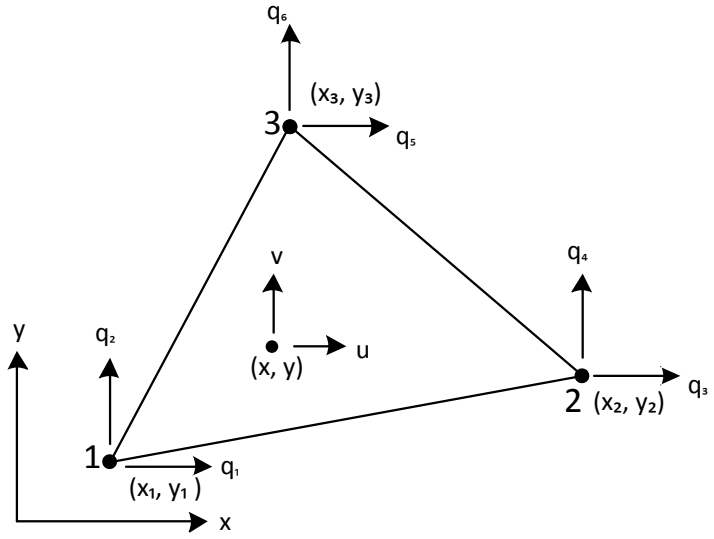

Figure 3.7: Constant Strain Triangle (CST) used for in-plane strain measurement

Given the position and deformation for three points in the contact patch, the longitudinal (ϵ_x) and lateral strain (ϵ_y) and shear (γ_{xy}) is calculated as in Equation 3.1 where A is the area of the triangle used. The distance between point A and point B is given by x_{AB} and y_{AB} in the horizontal and vertical direction, respectively. The deformation of each node is given by u and v. Four triangles sharing a common point are averaged to give the average longitudinal and lateral strain around a point.

$$\begin{Bmatrix} \epsilon_x \\ \epsilon_y \\ \gamma_{xy} \end{Bmatrix} = \frac{1}{2A} \begin{bmatrix} y_{23} & 0 & y_{31} & 0 & y_{12} & 0 \\ 0 & x_{32} & 0 & x_{13} & 0 & x_{21} \\ x_{32} & y_{23} & x_{13} & y_{31} & x_{21} & y_{12} \end{bmatrix} \begin{Bmatrix} u_1 \\ v_1 \\ u_2 \\ v_2 \\ u_3 \\ v_3 \end{Bmatrix} \tag{3.1}$$

3.3.2 Calibration

Due to the cameras wide baseline and small focal length of the lens, distortion is inherent and thus needs to be removed. Radial distortion warps the image such that straight lines within the image are warped when projected onto the image sensor, this effect is more pronounced at the edges. It must be noted that the oval shape of the point cloud is not the shape of the contact patch but rather the points which are mutually seen by the left and the right camera.

3.3.3 Algorithm settings

The subset window used to correlate regions between two images has a noticeable effect on the 3D point clouds produced. The effects of subset size and spacing is discussed.

Subset size

Deformation and strain measurement is computed by correlating features between images. The 1024 x 1280 pixel resolution reference image is searched for unique patterns with a window of a set subset size. The larger this subset size (in pixels), the more unique the window which is searched for and, therefore, the better the correlation. There is a limit to how much the subset size can be increased as a large window search is computationally expensive. It is assumed that the strain in the subset is constant thus the larger the region the higher the chance that points will not be detected due to varying strain. The effects of subset size on images taken of the inside of the tyre is shown in Figure 3.8. The same image pair, left and right image, were used for the reference and current state to note the effects of subset size on the produced 3D image. Keeping the subset spacing constant, the subset size was incrementally increased to find a suitable subset size based on the number of points detected. An ideal subset size in this case was seen to be a size of 70 pixels. Figure 3.8 shows that neither too large or too small of a subset size is beneficial in order to correlate the majority of the captured region.

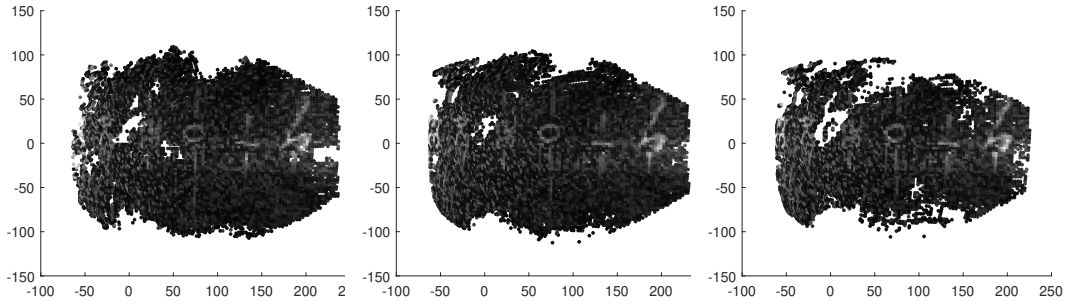

(a) Subset size = 35, Spacing= 7 (No. of Points = 9233)

(b) Subset size = 70, Spacing= 7 (No. of Points = 10 776)

(c) Subset size = 100, Spacing= 7 (No. of Points = 8688)

Figure 3.8: The effect of subset size on an image captured of the inner surface contact patch

Subset spacing

The subset spacing is the distance between the centres of neighbouring subsets of points. A smaller subset spacing yields more correlated DIC points thus a higher spatial resolution and more points reached towards the edges of the images. The same region was captured with the different subset spacings while keeping the subset size constant. Its effects can be seen in Figure 3.9. A subset spacing of 5 pixels ideally captures majority of the points within the captured region. Too large of a subset spacing is seen to cause large regions of lost points. Using a particularly small subset size will increase the computational time and memory requirement thus keeping this parameter at a moderate size of 5 pixels is deemed suitable.

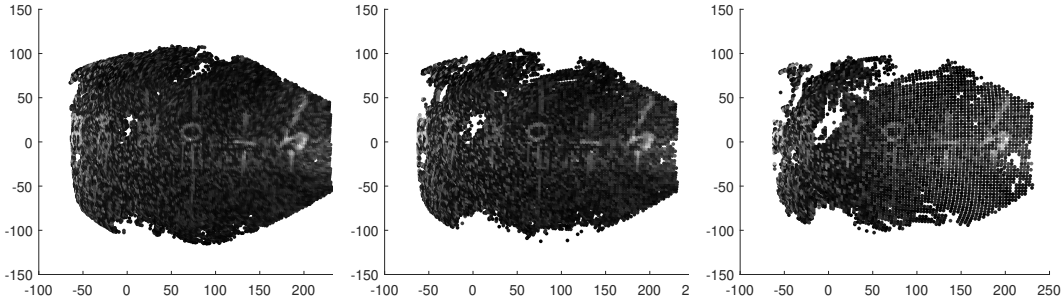

(a) Spacing= 5,
Subset size = 70
(No. of Points = 24 216)

(b) Spacing= 7,
Subset size = 70
(No. of Points = 10 776)

(c) Spacing= 9,
Subset size = 70
(No. of Points = 5459)

Figure 3.9: The effect of subset spacing on an image captured of the inner surface contact patch

Chapter 4

Full-field strain comparison between a passenger car tyre and an agricultural tyre

Strain within the contact patch is dependent on several factors, one being the tyre structure. Agricultural tyres have a greatly different tyre structure to that of a passenger car tyre, such a tyre structure poses large strain concentrations in the region of their large lugs. This effect results in a strain field which is largely non-homogeneous with very abrupt changes. In this chapter, initial tests are conducted on both a smooth treaded tyre and a large lugged tyre, to demonstrate the strain field without the effect of tyre structure. Both the investigated tyres are radial tyres and therefore differences due to the tread structures will be investigated. The two tyres were statically tested with T2Cam on a static tyre test rig. The smooth treaded and large lug tyre is shown in Figure 4.1.

(a) Michelin LTX A/T2 LT235/85/R16 **(b)** Trelleborg TM700 280/70R16 TL

Figure 4.1: Smooth treaded and large lug tyre used for comparing the effect of tyre structure

4.1 Inner surface strain of smooth treaded tyre under static loads

A static tyre test rig (STTR) was used to statically load the test tyres. Statically testing allows for well-controlled testing which can give valuable insight before moving to dynamic testing. The STTR, as shown in Figure 4.2, allows the fixed tyre to be deformed longitudinally, laterally, vertically and certain combinations of the three directions with an hydraulically actuated flat bed. For the purpose of this analysis, only the vertical loading is discussed.

Figure 4.2: STTR in longitudinal and vertical loading position with smooth treaded tyre installed

The test tyre was vertically loaded at 3 Bar with incremental increases in vertical load, the strain distributions at discrete loadings is shown in Figure 4.3. The full-field longitudinal (top) and lateral (bottom) strain is shown with the vertical load given as a percentage of the load index at that particular test pressure.

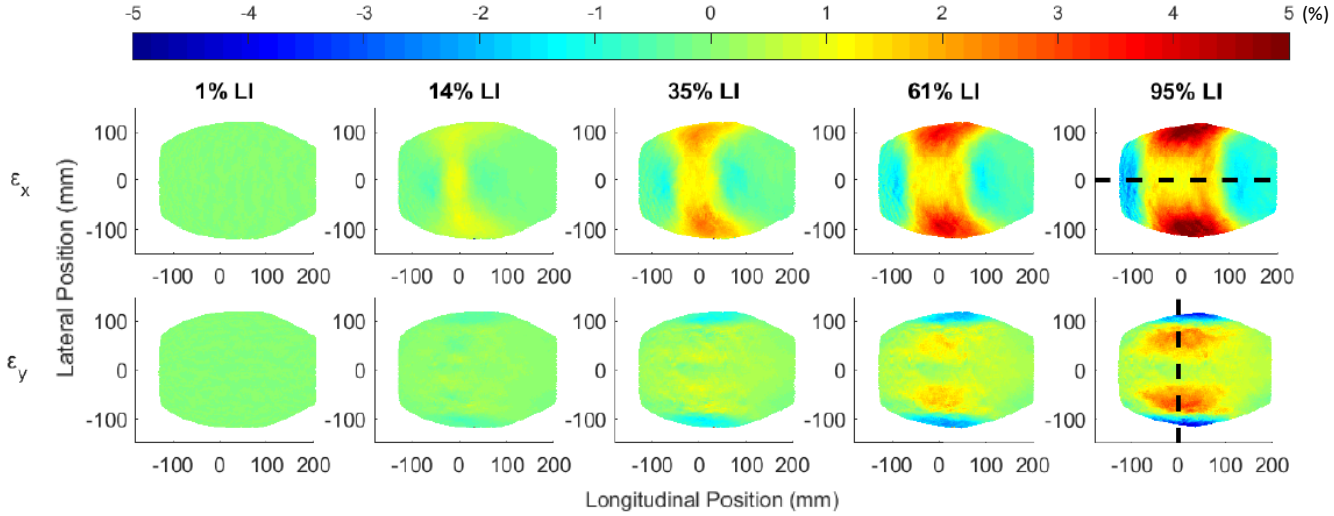

Figure 4.3: Discrete longitudinal and lateral strain of a vertical loading test on smooth treaded tyre (3 Bar)

For the longitudinal strain, an increase in load causes strain concentrations at the lateral ends of the contact patch. The contact patch is tensed along the longitudinal centreline,

with this area widening with increase in load. To the left and right of the centre of the contact patch, an area of compression is seen which increases in magnitude with increase in vertical load but not to the same degree as the regions in tension. For the lateral strain, the contact patch is predominately in tension with two prominent tension bands increasing in magnitude on either side of the longitudinal axis, with increase in vertical load.

The strain distribution along a length of the contact patch can be used to demonstrate the strain's sensitivity to loading. The longitudinal strain along the longitudinal axis and the lateral strain along the lateral axis are shown in Figure 4.4 at increasing vertical loads. For the longitudinal strain, an initial increase in vertical load resulted in an increase in tension and compression peak values. Up to a load of $\approx 40\%$ LI, the tension peaks no longer increases and remain constant regardless of increase in vertical load. The length of the tensioned area, however, increases which could be an effect related to the friction coefficient of the test surface. The saturation level may be dictated by the friction of the test surface and warrants further investigation in future studies. The compression peaks of the longitudinal strain continue to increase, this increasing distance between the two compression peaks can be used as an indication of increase in contact length with increase in load.

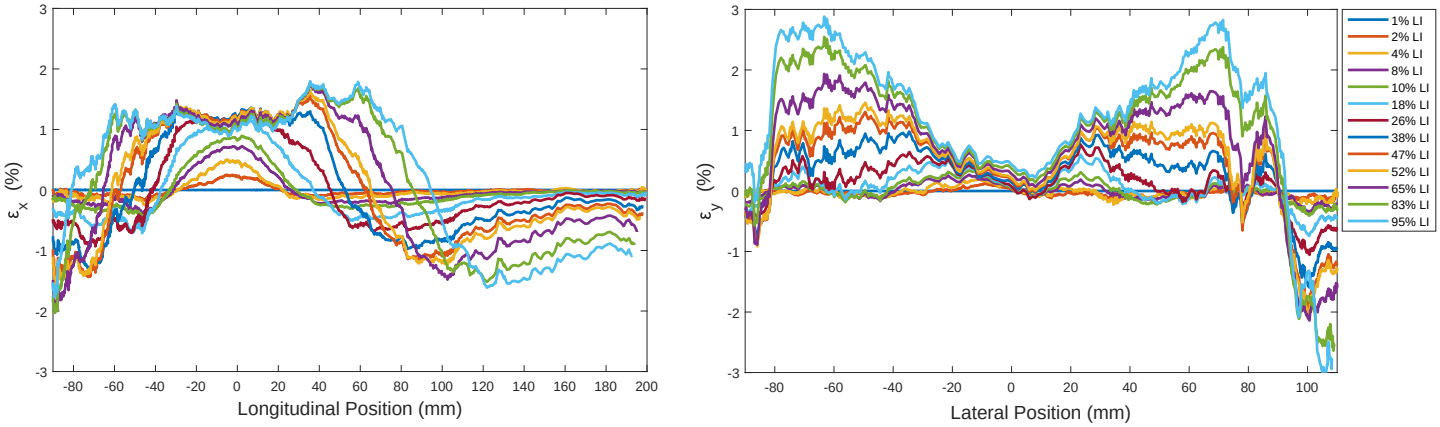

(a) **(b)**

Figure 4.4: Discrete longitudinal and lateral strain measurement along the centreline from a vertical loading test on smooth treaded tyre (3 Bar)

The lateral strain was not seen to saturate at higher loads. The two tension peaks continue to increase with load while the centre of the contact patch remains fairly unaffected with increase in load. Regions of compression are seen to appear at the edges of the lateral axis however the full extent of this region was not captured. It should be noted that the strain trends of a smooth treaded tyre are relatively smooth in nature with no abrupt changes between different locations within the contact patch. Thus, the small treads indeed show little effect on the contact patch strain.

Similar results were seen by Lee et al. (2015), where it was noted that the strain in the tension region did not deviate with various loads as the tyre contacts the road and forms a horizontal peak in a static tyre. The maximum compression strain showed the most correlation with increase in test load while the maximum tensile strains tended to be saturated or decrease as test loads increased above a certain point.

4.2 Inner surface strain of an agricultural tyre under static loads

A static test, as performed by Feldesi et al. (2020), of the same agricultural tyre used in this study is used as a comparison to the smooth treaded tyre strain results. The tyre was tested using the same STTR as seen in Figure 4.2. The longitudinal and lateral strain for a vertical test of the agricultural tyre (at 2.0 Bar) is shown in Figure 4.5. Similar to the smooth tread tyre, strain concentrations appear at the lateral ends of the longitudinal strain. These appear along the lug locations. With increase in load, the strain concentrations appear along the whole length of the lug. Compression peaks are seen at the beginning and end of the contact patch.

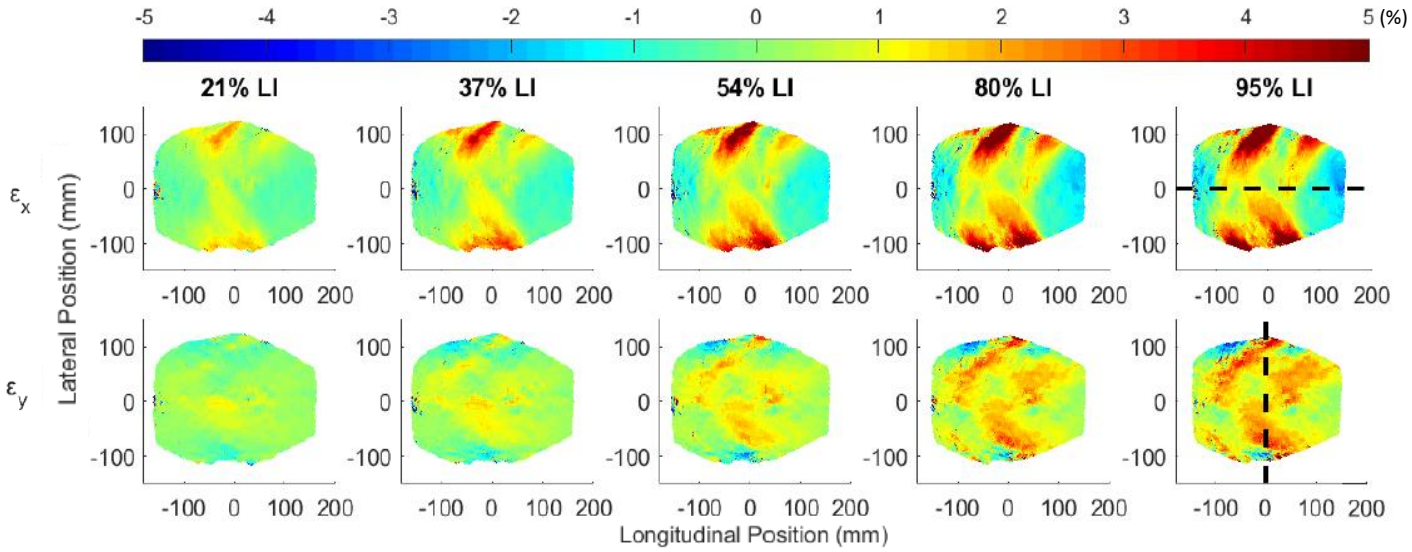

Figure 4.5: Discrete longitudinal and lateral strain vertical loading test on agricultural tyre (2 Bar)

The lateral strain is predominately in tension with increasing tension regions appearing along the whole length of the lug and not primarily at the edges. The longitudinal strain and the lateral strain along the same locations as the smooth tread tyre are shown in Figure 4.6 with increase in vertical load. It appears that the agricultural tyre too has areas of no dependence of vertical load when it surpasses a certain vertical load. Signs of tyre saturation can also be seen towards higher load indexes.

The influence of tyre structure is seen to have a large effect on the contact patch strain. Strain analysis thus differs between different tyre types. Determining the individual influence of each factor can be challenging with tyre structure having such a large effect. Without effects from tyre structure, smooth tread tyre measurements can be extracted from a single image instance. This is due to the outer contact patch only varying when driving conditions are changed. Keeping driving conditions constant will result in constantly varying strain patterns in an agricultural tyre due to the large lugs having changing contact with the road.

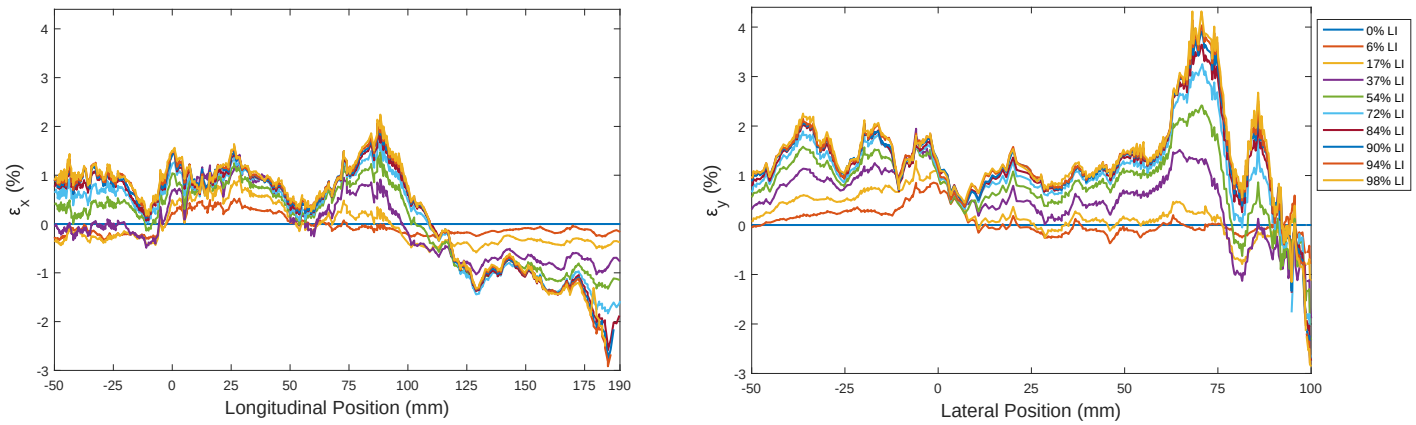

(a) **(b)**

Figure 4.6: Discrete longitudinal and lateral strain measurement along centreline for vertical loading test on agricultural tyre (2 Bar)

4.3 Conclusion

The same static vertical test was performed on a smooth treaded tyre (Figure 4.3) and a large lugged tyre (Figure 4.6). Large differences were seen in the strain patterns produced, indicating that the lugs certainly have a significant effect. Areas of strain concentration for the smooth treaded tyre were seen to appear at the lateral edges of the tyre for longitudinal strain and appeared for the lateral strain along two bands at a positive and negative lateral position. A large lugged tyre also experiences an increase in strain towards the edges. The highest concentrations would occur at the edges of the lugs, with strain increasing along the lengths of the lugs with increase in vertical load.

Strain trends and magnitudes are thus greatly dependent on the test tyre and its structure. Point measurements placed at different circumferential regions in a smooth treaded tyre will deform and strain in a fairly similar way thus producing similar results. However, within the contact patch of an agricultural tyre there are several regions which act differently in the way they deform and strain. Placement of point measurements inside of an agricultural tyre thus requires prior knowledge of the areas of high strain within the contact patch. Agricultural tyres require a full-field approach in order to select and place suitable sensors for point measurement. The static results conducted by Feldesi et al. (2020) will be used to find suitable locations for strain gauges for better sensitivity of strain measurement in the next chapter.

Chapter 5

Point strain measurement via the inside tyre surface

Without a way to calculate the theoretical strain of the tyre, strain gauges were selected to provide a comparison measurement with both point and full-field strain measurement having their advantages and disadvantages. Many studies perform FEM analysis prior to strain gauge placement. In this study the placement of the strain gauges will be based on static test results available on the test tyre, as conducted by Feldesi et al. (2020). Tests will then be done with both measurements and compared to the camera system. The sampling rate for strain gauges are favourable thus giving valuable information when paired with the camera system.

5.1 Strain gauge location

As determined in Chapter 4, the lugs of an agricultural tyre have a significant effect on the strain fields produced. Strain concentrations appeared around the lug locations and locations between the lugs would experience little strain. In order for strain gauges to show meaningful results, they should be placed at regions of high strain-to-noise ratio. Many previous studies have made use of FEM models to find a location for point measurements based on high strain-to-noise ratios and to measure changes in slip angle and/or camber. The location of the strain gauges in this study was selected based on the static results of the test tyre performed by Feldesi et al. (2020) during various testing configurations. The strain patterns measured by the tyre is dependent on the tyre structure, therefore, the trends seen on a passenger car tyre versus agricultural tyre will be different. The optimal location thus differs and is discussed below.

5.1.1 Static agricultural tyre

The test tyre was tested statically in numerous configurations on the same flat-bed test rig discussed in Chapter 4. The effects of inflation pressure and load was used to find regions of high strain suitable for strain gauge placement for this specific tyre. The tyre was tested up to its recommended load index to explore strain patterns at maximum loading. The static test was performed with the camera system focused on the same region throughout testing, therefore, the strain due to tyre structure will remain unchanged.

The inflation test is used to determine the location of the tread blocks which will be locations of high strain. The longitudinal and lateral strain for an increase in inflation pressure is given in Figure 5.1, where the reference state was an uninflated tyre. As the inflation pressure increases within the tyre's working pressure range, strain concentrations increase around the location of tread blocks in the longitudinal strain. The high strain experienced along the lateral edges of the lateral strain is due to the tyre weighted laterally as positioned on the STTR. The lateral strain experiences increased strain in between tread blocks, with a subsequent increase in inflation pressure. Therefore, this will increase the maximum tension and compression for other testing cases at higher pressures. The influence of other factors on the strain will be then used to find an optimal location of point measurements with the knowledge that strain at peak points increases with inflation pressure.

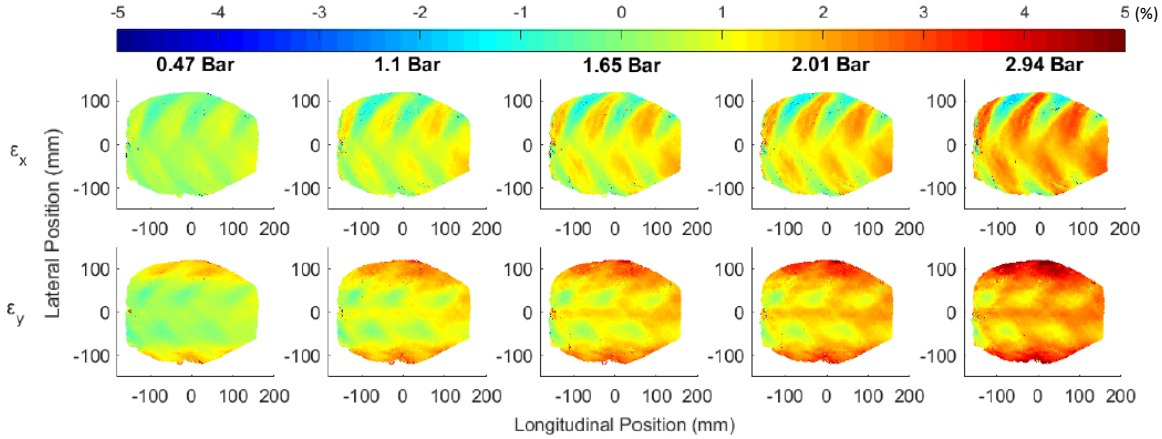

Figure 5.1: Discrete longitudinal and lateral strain with increase in inflation pressure on an agricultural tyre

With the knowledge of the effect of inflation pressure, the effect of other loading conditions is used to determine regions of high strain from loading. A vertical test at 2.0 Bar is discussed where the tyre inflated to 2.0 Bar is the reference state. The longitudinal and lateral strain with increase in vertical load is given in Figure 5.2.

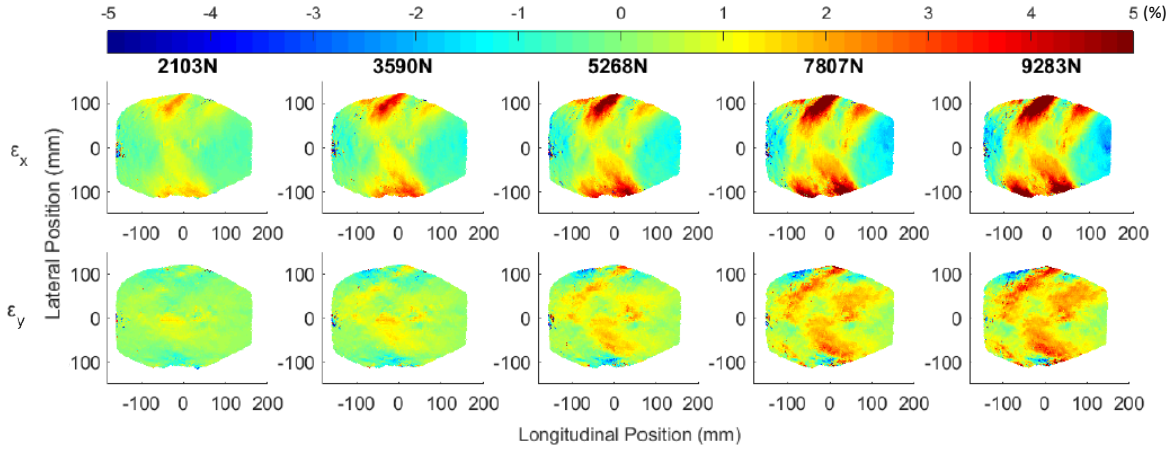

Figure 5.2: Discrete longitudinal and lateral strain with increase in vertical load on an agricultural tyre (2 Bar)

The peak strains occur at the edges of the contact patch. An increase in vertical load causes this peak strain to increase and the strain along the length of the lug to increase until a new lug also makes contact with the test surface. Along the length of the lugs are locations suitable for point strain gauge placement. The strain gauge placement was done from static test data which lacks phenomena only occurring in dynamic testing, therefore, the initial placement may be useful to understand the comparison of point to full-field measurements but may not produce results which solely can be used to predict tyre parameters. The chosen locations will be analysed, and then full-field measurements will be used to suggest possibilities for new locations to predict parameters such as slip angle. Another benefit of full-field measurement is the ability to find and change the optimal location for analysis after testing is completed.

A region of high strain was identified from the vertical loading and three strain gauges were placed along the length of the region. Their positions are shown in Figure 5.3.

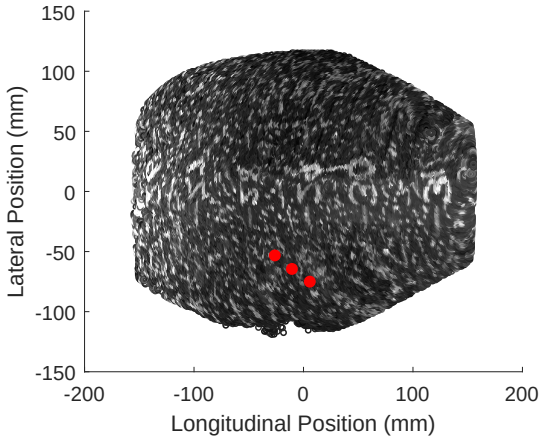

Figure 5.3: Point location for placement of strain gauges on inner surface of an agricultural tyre

The vertical load and inflation pressure was seen to have a dominant effect on the contact patch strain. Therefore, the point locations were based primarily from these results. The location of the strain gauges on a 50% LI vertically loaded tyre, under longitudinal and lateral loads is shown in Figure 5.4. The reference state for the lateral and longitudinal tests was an inflated vertically loaded state. This highlights the changes in strain relative to this state and removes the strain imposed on the tyre due to the vertical load, which has a dominant effect.

While the effects of longitudinal and lateral strain are less than that of inflation and vertical load, the point measurement location is suitable to detect changes in longitudinal and lateral loads. The strain gauges were attached to the tyre when it was uninflated and unloaded. Therefore, all strain is due to inflation pressure and loading conditions and temperature effects. Once the tyre was mounted onto the test rig, the strain gauges were recorded for the reference strain value and this was then removed from the strain experienced during testing to remove the effect of inflation pressure.

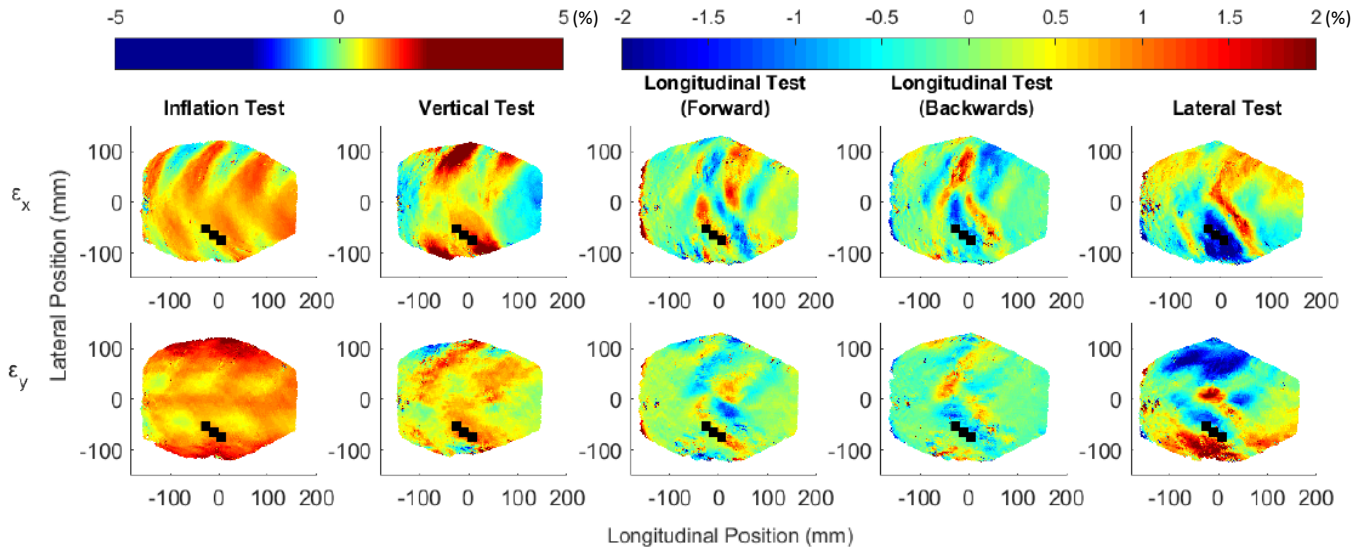

Figure 5.4: Inflation test, Vertical Test, Longitudinal Test (forward), Longitudinal Test (backward) and Lateral test on an agricultural tyre (2.0 Bar)

5.2 Strain gauge wiring configurations

Measurement of rubber is not a common application for strain gauges, even less so on a curved surface such as the inside of a tyre. Strain gauges can be wired into numerous configurations in order to achieve different measurements or mitigate the effects of unwanted variables. Given the structure of the tyre, many of these configurations are not possible with many requiring symmetrical application. Strain gauges come with many difficulties, however, for short-term testing, these can be manageable.

Keeping all tests to short intervals will exclude the need for temperature compensation. However, should the tyre be tested for prolonged periods of time, this will be necessary. To achieve this, a dummy gauge is used. The dummy gauge, when placed on an area of no strain but within the same testing environment, will remove the strain caused by temperature. There are limited options for placing a dummy gauge and within close proximity to the full configuration. Strain is experienced throughout the tyre and thus a dummy gauge will not be effective within a tyre.

The two possible strain gauge configurations are that of a quarter and a half bridge as shown in Figure 5.5. As seen in Figure 5.4, both longitudinal and lateral peak strains appear at the selected gauge locations, therefore, a strain gauge which can measure both directions is suitable. The quarter bridge (Figure 5.5(a)) can be used for both the longitudinal and lateral direction depending on the position of the gauge. This configuration does not have temperature compensation. Inclusion of a second gauge (Figure 5.5(b)), placed orthogonal to the first, will provide temperature compensation, however, requires knowledge of the poisson ratio. The poisson ratio can be estimated to be 0.5 for rubber, however, this can also be estimated by the longitudinal and lateral full-field measurement at a unit area.

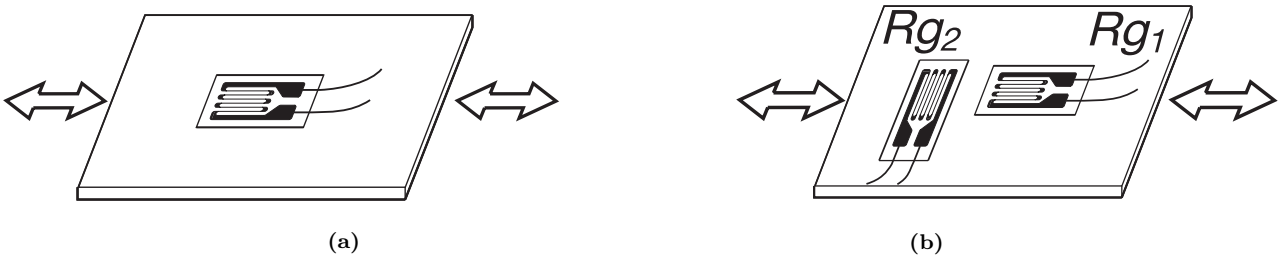

(a) **(b)**

Figure 5.5: (a) Quarter and (b) Half bridge configuration

The strain gauges selected for this study are Micro-Measurements EP-08-125TM-350 strain gauges (Figure 5.6). From static results, it was noted that strains in the agricultural tyre will not exceed ±10% strain. Catering for high strains, the gauge has a strain range of ±20% and a temperature range of -75° to 205°C. The small size of the sensor is 5.46mm × 8.51mm. The gauge is sensitive in both the horizontal and vertical direction where the strain gauge is passive perpendicular to the length of the coil pattern and active along the length of the coils.

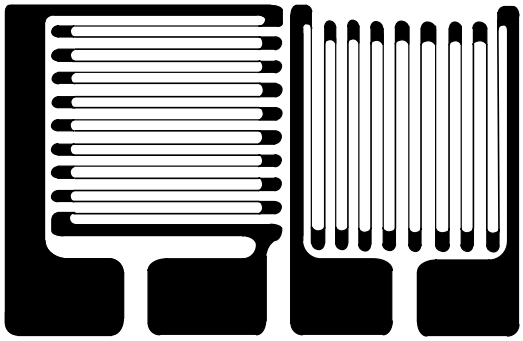

Figure 5.6: Micro-Measurements EP-08-125TM-350 strain gauge

In order to ensure accurate measurement of tyre strain, the correct bonding method will need to be selected. A wide range of adhesives are available with varying operating temperature ranges, elongation capabilities and shelf life. Few adhesives have properties which perfectly match the sensors to which it is bonding to. The bonding method is an important component of the strain gauge installation to ensure proper use of the strain sensor and to avoid debonding of the sensor from the measured surface. For this application an adhesive with a relatively high elongation is desirable due to the flexible nature of the tyre. Many of the adhesives available have a limited elongation of ±3% thus a special-purpose adhesive was required to match the ±20% elongation capabilities of the strain gauge. Without a strong bonding between the strain gauge and the rubber will result in debonding over repeated loadings. The adhesive used was a Micro-Measurements M-Bond A-12 Adhesive which also could reach ± 20 % strain.

The double strain gauges were selected so configurations and directions could be easily changed, once installed. Perfectly orthogonal placement of the strain gauges will be difficult to achieve thus the double strain gauges also removes error due to application. The

selected strain gauges were temperature self-compensated. However, as noted, testing did not last long thus, temperature would not increase above the manufacturers recommended range.

5.3 Installed strain gauges

The three point measurements were added to the inside tyre surface at the locations indicated in Figure 5.3. Lead wires were added the strain gauges as seen in Figure 5.7, which were later wired to the correct configuration. A lateral and longitudinal quarter bridge and a half bridge configuration was used to have a combination of the three measurements. The correct processes were followed as recommended by the adhesive manufacturer. The inner surface of the tyre was textured which could not easily be sanded down. The inner surface of the tyre does not guarantee a perfect adhesion and thus this must be considered when selecting strain gauges.

Figure 5.7: Installed inner surface strain gauges

Chapter 6

Experimental Work and Results

Strain of the inside tyre surface is measured using both point and full-field measurement systems, namely strain gauges and T2Cam. The test tyre was dynamically tested on a drum roller. Straight-line and cornering conditions were tested at varying loads, inflation pressures and slip angles.

6.1 Artificially strained images

Prior to placing T2Cam inside the tyre, the camera system's accuracy is tested. Unfortunately, within this study, rubber could not be strained to a known value and then tested by T2Cam. Rather, a speckle pattern as seen in Figure 6.1 is printed on paper at different known sizes, mimicking a strained surface. The print outs are placed on a fixed clipboard in front of the cameras at the same distance the tyre surface would be from the cameras when inside the tyre.

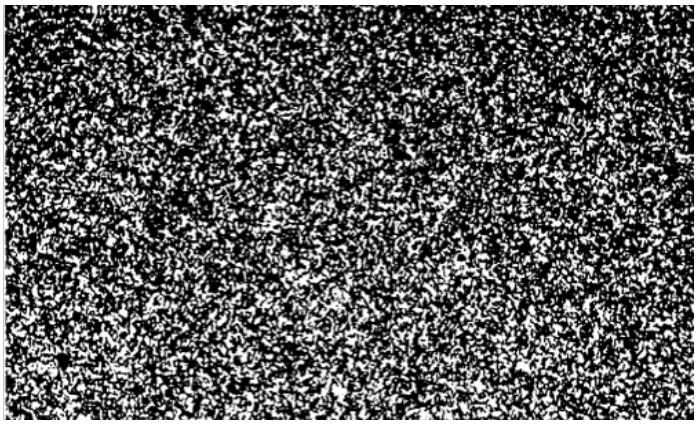

Figure 6.1: Speckle pattern used to test accuracy of strain measurements

This process is not fully representative of the environment in which the cameras will be tested. The printing process also causes some effects which may affect the results, however, it can give some indication of accuracy. Unfortunately, the speckle pattern was tested at much larger strain values than was experienced during testing. The pattern was strained in one direction as well as both directions together as seen by the animation to the left of

Figure 6.2 and 6.3. Edges effects are seen in Figure 6.2 which occur as the pattern abruptly disappears, these high strains are excluded when calculating the average strain. The error is below 10% for the shown cases, the system is known to have an error of 0.5% as shown by Feldesi et al. (2019). The error is believed to be caused by the printing process which may not be scaled correctly.

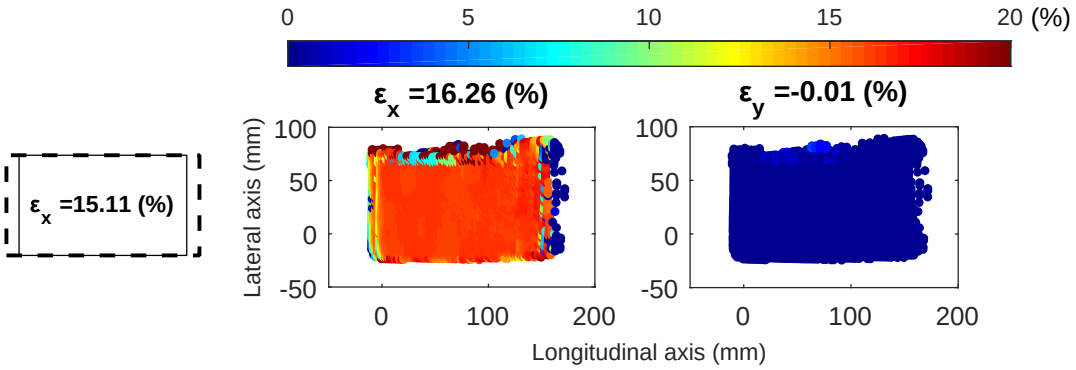

Figure 6.2: Surface after horizontal strain

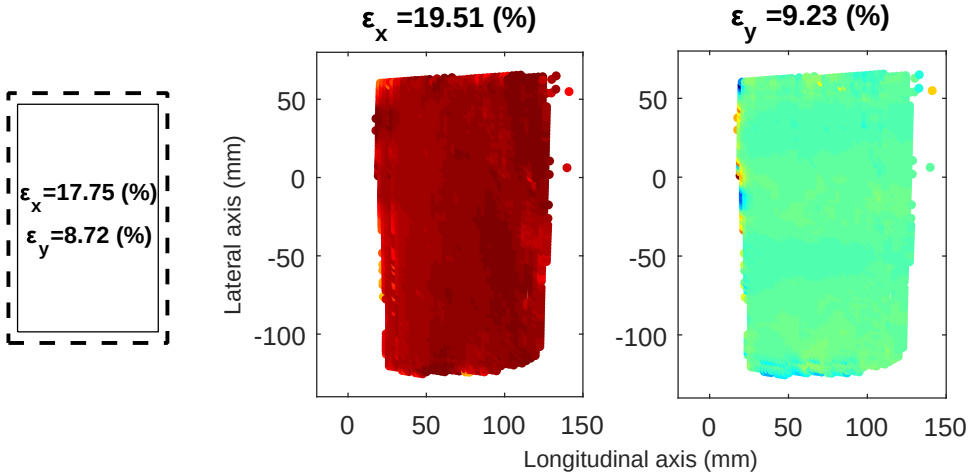

Figure 6.3: Surface after horizontal and vertical strain

6.2 Test Setup

Dynamic and static test rigs are favourable in terms of repeatability and controllability in comparison to road tests. The tyre was tested for straight line rolling and cornering conditions to analyse strain characteristics relating to tyre dynamics. The tyre working conditions will be varied to find the influence of inflation pressure, vertical load and slip angle.

6.2.1 Strain gauges

With the installed strain gauges capable for high elongations - the gauges will be able to measure what is experienced by the rubber without local stiffening. Without much

knowledge of strain results on normal roads with a large lug tyre, results between the strain gauges and T2Cam will be compared.

6.2.2 Drum roller

The drum roller provides a testing environment to test tyres at varying conditions. Drum testing, however, cannot allow for the full strain distribution due to the rounded surface. The relatively small 0.8m radius curvature of the drum has an influence on the deformation of the tyre however this effect can be considered small in comparison to the benefit gained using the well-controlled laboratory environment. The complete test setup is seen in Figure 6.4.

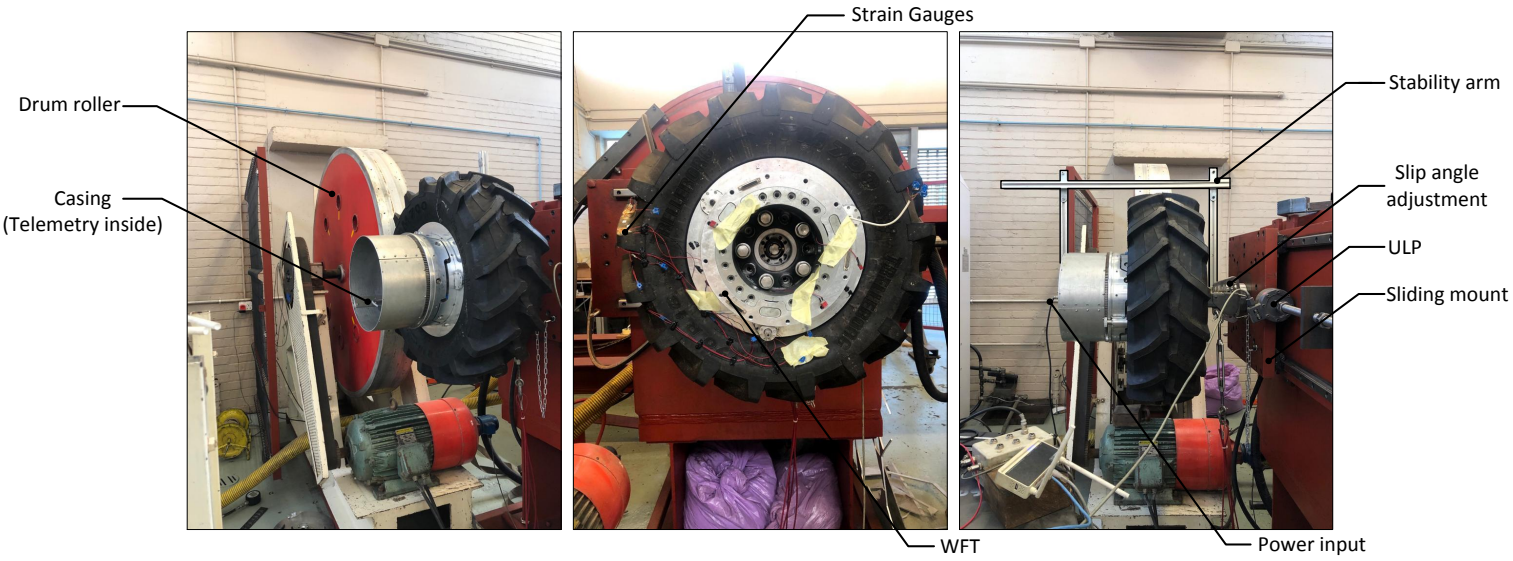

Figure 6.4: Dynamic test setup with agricultural tyre installed

The dynamic setup is suitable for determining strain characteristics relating to tyre dynamics as well as tyre-road relationship, the latter will be performed in future studies. Including abrasive paper on the drum surface can help determine the impact of tyre-road interface on the tyre performance.

The test tyre is fixed on a sliding mount. This sliding mount can be moved towards and away from the drum roller. The tyre can be loaded onto the drum by pushing or pulling the mount. The fixed mount of the tyre can be rotated to vary the slip angle. The pivot of the mount can be locked into different slots which provide different slip angles. The range for the slip angles achievable is -15° to 15°. The vertical load of the tyre was measured with a Universal Low-Profile (ULP) loadcell. The ULP was installed on the rod between the sliding mount and where force is applied. A WFT was included in the test setup as the telemetry, which measured the strain gauge signal, was designed to bolt onto the tyre through the WFT. The force measurement was not used from the WFT for post-processing analysis.

To keep the cameras at a fixed position within the rotating tyre, the outer sun gear needs

to be kept stationary. This, along with the wheel encoder, is fixed with a stability arm to prevent rotation. The stability arm is seen in Figure 6.4. Before testing, the cameras are aligned with the centre of the contact patch against the drum. For this, the stability arm is removed so that the cameras can move freely. The outside of the tyre has matching markings to the inner surface at 10° increments. The tyre's outer 0° incremental mark is aligned with the drum and the cameras are moved to find the image pair which results in the inner 0° mark appearing in the centre of the contact patch. The planetary gear is then secured to the sun gear so that the cameras position is fixed and will remain fixed when the tyre rotates. However, after post-processing, it was noted that the cameras were not perfectly focused on the centre of the contact patch and this was due to the outer and inner 0° markings not being fully aligned which caused the cameras to be off centre. This will be seen in the post-processed results.

6.2.3 Data capture

A simplified schematic of the test setup, as seen in Figure 6.4, is given in Figure 6.5 in order to explain the data capture procedure used during testing. The test setup includes three sampling devices, each of which is indicated in Figure 6.5. A telemetry is used to record the strain gauges and wheel encoder signal, a static Data Acquisition (DAQ) is used to measure the applied vertical load from the ULP and a Mintbox inside the tyre which records the images captured by the cameras. The telemetry and the DAQ is synchronised by sharing the same electric trigger signal. With T2Cam within a tyre, there is a possibility of triggering image captures via wifi, however, there were uncertainties to whether this would have an adverse time delay.

The test setup's trigger sequence is indicated in Figure 6.5. The testing procedure is briefly explained as this was done in a particular order to be able to aptly synchronise the T2Cam images (Trigger sequence 2) with the other trigger sequence (Trigger sequence 1). Testing began with the drum unloaded and stationary. The drum is started and once the drum gained constant speed, the telemetry and DAQ were triggered to begin sampling (Trigger sequence 1). Up to now, the tyre remains stationary and therefore the wheel encoder measurement as recorded by the telemetry remains at a constant value. The tyre is loaded onto the drum, and the tyre begins to rotate as it makes contact with the rotating drum. The initial motion of the tyre can be detected by a sudden change in the wheel encoder reading. This first change in reading can be synchronised with the first image taken by T2Cam. Once T2Cam is powered up, image capture is triggered with change in rotation (Trigger sequence 2) therefore images will be recorded the moment that the tyre begins to rotate.

Due to the motor limitations for the drum, the tyre was not loaded to a desired load but rather until the drum's rotation halted. Once the drum rotation halts, all the sensors recording was ended and data was captured.

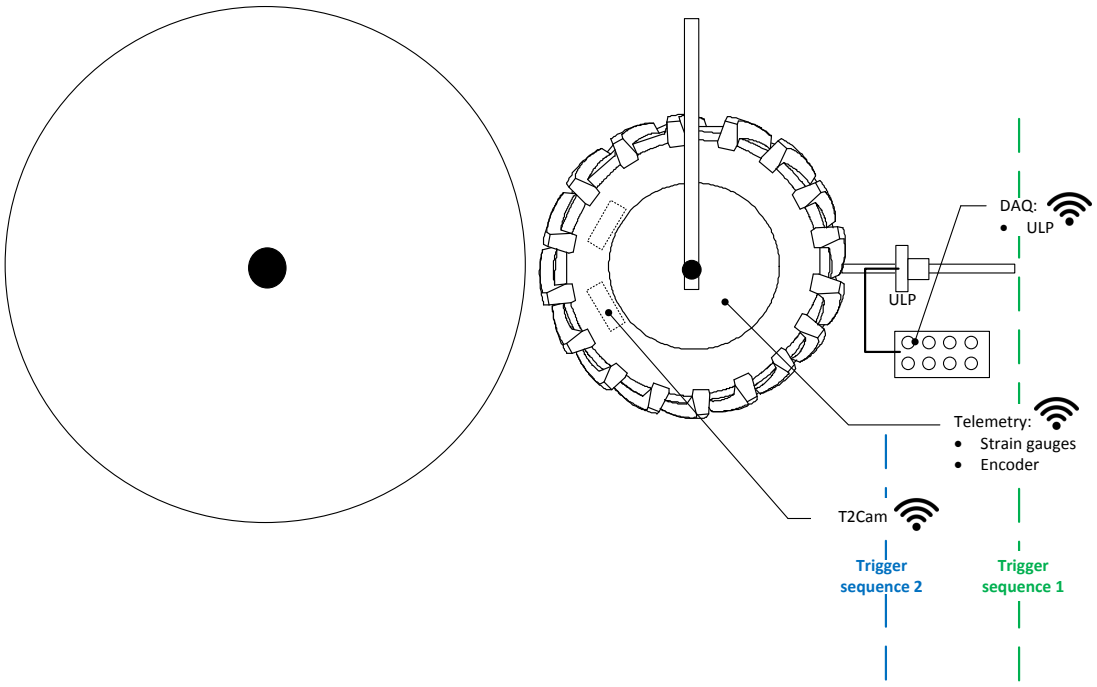

Figure 6.5: Trigger sequence used during testing

6.3 Data post-processing

Before the results are presented, the processes to sync and analyse the data is explained.

6.3.1 Syncing Data

The syncing of the data became a challenging task due to some issues that only became apparent once testing was finished. The first syncing was between the two triggering sequences namely T2Cam to the DAQ and Telemetry. The DAQ and Telemetry was sampled at 1000Hz while T2Cam is to ideally record 172 images per revolution. T2Cam was seen to miss images and this was due to two reasons. The first reason was caused by the rotational speed, while the starting speed was set to a low speed of $5km/h$ this was realised to be too fast for T2Cam to be triggered and capture images for each 172 teeth. If the cameras were triggered while still capturing the previous image, that trigger would be ignored and the next image would not be taken. Secondly, it was seen after testing that the ring holding the proximity switch, inside of the tyre, was warped. Therefore, the proximity switch moved further away from the teeth at certain regions and thus resulted in a dead region which was not captured by T2Cam.

An example of the missed regions is seen in Figure 6.6. The colour points are useable images which means that the left and right camera captured the particular region and thus can be used for strain measurement. The black crosses are regions which were not captured by neither or one of the cameras and therefore, had to be discarded. Images which were not

captured within a time threshold of 20ms were discarded and are also indicated by a black cross in Figure 6.6.

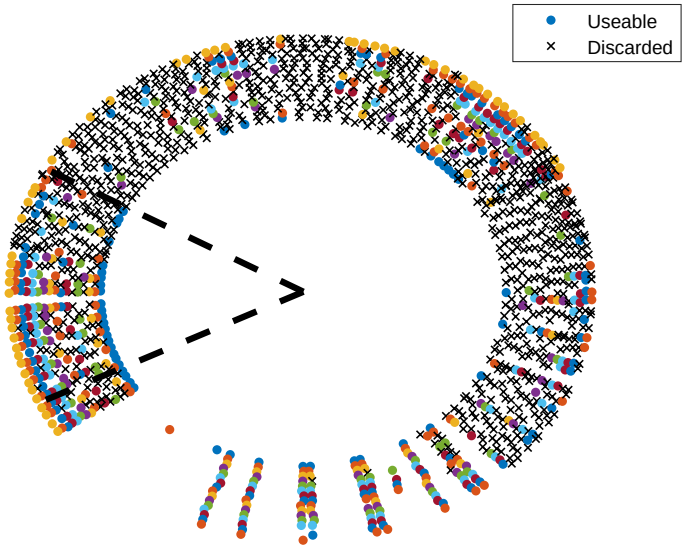

Figure 6.6: Images captured during testing

Towards the end of the test the drum speed would decrease and therefore, more images were captured and thus useable which can be seen for the last few revolutions. Overall, the issues resulted in a very low sampling rate which is not ideal in order to be able to compare results to 1000Hz sampled strain gauges. Several improvements are needed for the current triggering system which will ameliorate the sampling rate. The syncing between the different measurements is discussed below with taking these issues experienced into consideration.

T2Cam and Telemetry

The two external recording devices, namely telemetry and DAQ, could not easily be synced with the internal recording device for T2Cam. T2Cam was synced to the telemetry, and therefore the DAQ, by making use of the wheel encoder measurement which is recorded by the telemetry. T2Cam and the telemetry are synced at the first instance in which the tyre begins rotation. Synchronisation was obtained by the motion recorded by the encoder and the initial image captured by T2Cam. This method proved not ideal, thus, an alternative method was used.

The on-board computer used for T2Cam is limited to 2000 images captured within one test due to a RAM limit. The original test procedure required the tyre to be stationary from the start of the test and for images to be recorded from the first moment of rotation. This was not ideal as this limited the amount of revolutions which could be recorded before the image limit was exceeded and the test run had to be ended. Because of this limit, the tyre load had to be constantly increased from the start to end of the test versus allowing the tyre to rotate at a constant load for a period of time before increasing to the next load

and then allowing for a transitional period between loads.

An alternative method was used which included adding an offset time to the T2Cam timestamps such that all images of the same region occurred at the same encoder value. This method, while only realised after post-processing, does not require the tyre to be stationary from the start. Tests can therefore be conducted such that measurements are only recorded when the tyre is rotating at the desired speed and set load. This method of testing would allow for better comparison between test results and therefore will be used in future works.

Reference and Current Images

The strain algorithm requires matching pairs of a reference and current state. During testing, the number of images captured was seen to be dependent on speed. With slower speeds, more images were taken and therefore, a better sampling resolution. The reference and the current images matching became a challenging task. The reference images were taken by manually rotating the tyre until a full revolution was captured. Manually rotating the tyre ensured that the movement was slow enough such that all teeth were triggered and all regions were captured. There was a dead region as seen by Figure 6.6, which occurred in both the reference and current tests, where no images were captured.

There was inconsistency with which regions were captured throughout the several revolutions. Asides from the dead region, there were no regions which were constantly captured or constantly missed. The reference test captured the most images possible and this then needed to be paired with the current state test images which had several of these regions missing. The wheel encoder measurement was used to match images that occurred at the same wheel encoder angle. This caused issues for comparing results between different tests because not all regions are captured with every revolution and thus limited data analysis greatly.

6.3.2 Comparing strain gauges and T2Cam measurement

The full-field and point strain could not be compared for the same region, as the region where the strain gauges were installed were obscured due to glue and lead wires. The region where the strain gauges were installed can be seen in Figure 6.7. A following lug sequence was thus used for full-field comparison, this region is indicated by the two dashed black lines in Figure 6.6. The strain measurement from T2Cam was compared to the strain gauges by tracking a point, captured continuously by T2Cam, which acted as a point measurement traveling through the contact patch. While T2Cam captures full-field strain in one image, this cannot be compared directly to the strain gauges due to the lug positions changing. Thus, it was needed to follow/track a similar lug region as a point measurement to compare the two measurements.

Figure 6.7: Inner surface strain gauges where silicon and lead wires can be seen to obscure the view of the installed region

The position of the strain gauges at the first image where they become visible by the cameras, is used as the starting location of the tracked point. Following a point between successively captured images is done using the 3D DIC algorithm where two images are used to find the new location of the tracked point at a 2D mode. This includes finding the displacement due to rotation (A) and the displacement due to the loading case (B), as seen in Figure 6.8. The combination of these two displacements will give the location to where the point moved to and the location of the next point strain measurement.

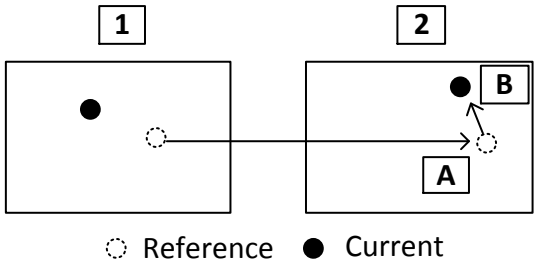

Figure 6.8: Method used to tracking a point from Frame 1 to Frame 2

Using this process, a chosen point is tracked through multiple images until no longer seen by the cameras as shown in Figure 6.9.

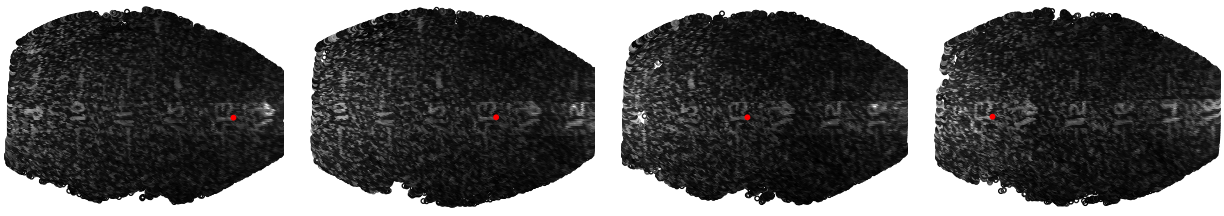

(a) Frame 1 **(b)** Frame 2 **(c)** Frame 3 **(d)** Frame 4

Figure 6.9: Tracking method used to track a point (red) from Frame 1 to Frame 4 as it moves from the right to the left of the contact patch

6.3.3 Degrees to mm

The T2Cam strain algorithm measures strain, per mm, within the contact patch while the strain gauges measures the strain, per degree, along the circumference. To compare these two measurements, the strains will be compared as strain per degree. Converting the T2Cam measurement from strain per mm to strain per degree is done using the following process. A point is placed at the centre of the contact patch and the wheel encoder measurement for this image set to 0° relative to the current encoder angle. The point is tracked in the consecutive image and its location and change in encoder angle is used to generate a function, as seen in Figure 6.10, over the consecutive images in which the point remains within the contact patch. This relationship will change slightly at different vertical loads, however, the change in radius will be small so this will be regarded as a small effect.

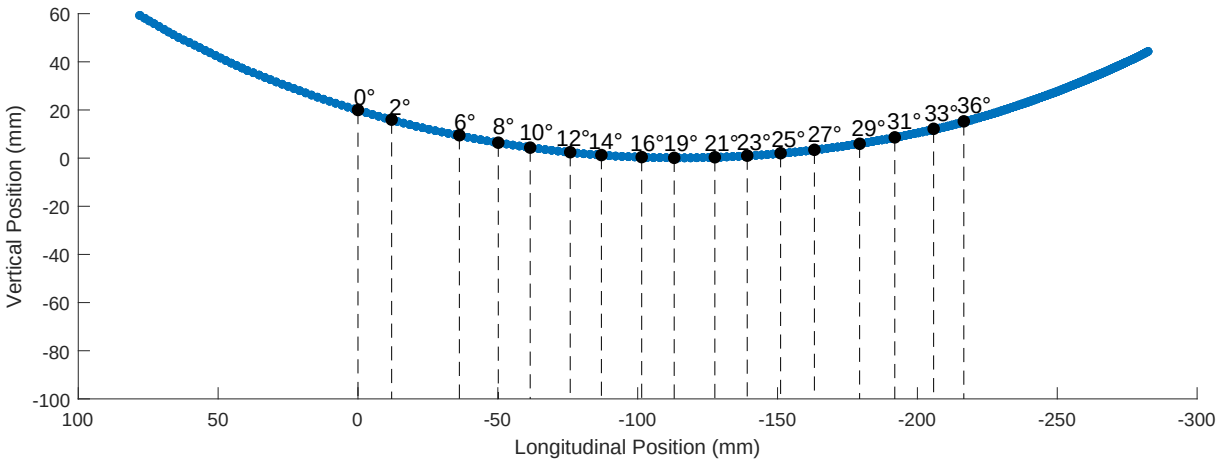

Figure 6.10: Method used to convert between millimetres to degrees

6.3.4 Dirt on lenses

The method to create a speckle pattern on the inner tyre surface was done with a white marker. During testing, the dried white ink would fall off the inner surface during large deformations. Some of this dirt fell onto the upward facing camera, as can be seen to the left of Figure 6.11. In between test runs, the tyre had to be deflated and one of the plugs were opened so that the camera lens could be cleaned with compressed air. Some of the images unfortunately captured images with the dirt but for majority of the cases it was towards to ends of the images and did not significantly affect the results. This can be prevented in the future by including a cover for the camera which will collect dirt while not appearing in the captured photo. Testing normally on a test vehicle will not be affected by this as the cameras orientation will be downwards.

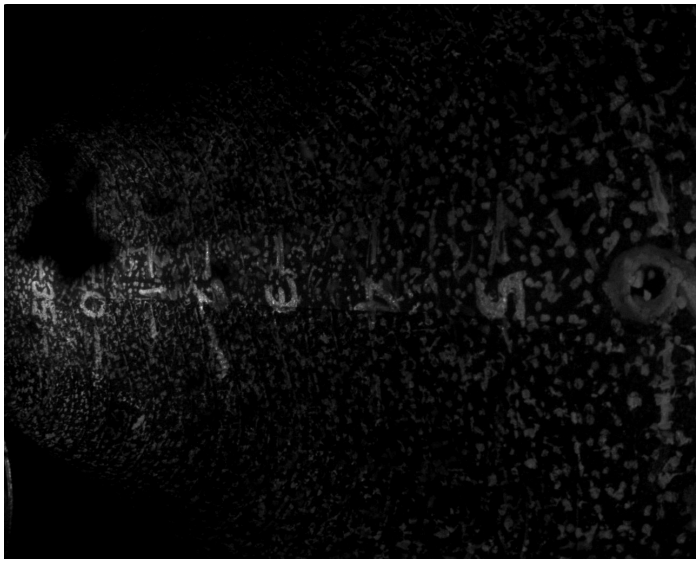

Figure 6.11: Dirt on upwards facing lens

6.4 Comparison of static tests on a flat and drum test surface

The agricultural tyre used in this study was previously statically tested with a flat bed. Testing statically on a flat surface versus dynamic drum testing are two largely different forms of tyre testing and cannot be directly compared. To bridge the gap, the agricultural tyre was first tested statically on the test drum to consider the effect the drum curvature will have on strain measurements.

The main difference between static tests and the dynamic drum tests lies in the contact region. With the round drum, the curvature decreases the size of the contact area. This will cause a difference between the area of the lugs in contact with the test surface and will be less for the drum surface as compared to the flat bed.

A tyre footprint test was conducted to find the difference in contact patch size between a flat bed and drum vertical test. The lugs, marked with black ink, was pressed onto the test surface which had a white sheet attached to it to imprint the contact shape and size. The tyre was statically loaded onto both test surfaces to load of 800N. The processed images of the contact patch footprint for the flat bed and drum is seen in Figure 6.12 (a) and (b) respectively. The size of the contact area was 2% smaller for the drum than the flat bed, which is a negligible difference. The drum curvature will therefore not drastically effect the loading of the tyre.

This test could, however, only be performed at a load of 800N. Larger discrepancies could be expected at higher loads due to a larger area of the tyre making contact with the test surface. These differences are assumed negligible and that the drum's curvature does not have a significant effect on the tyre strain and contact patch.

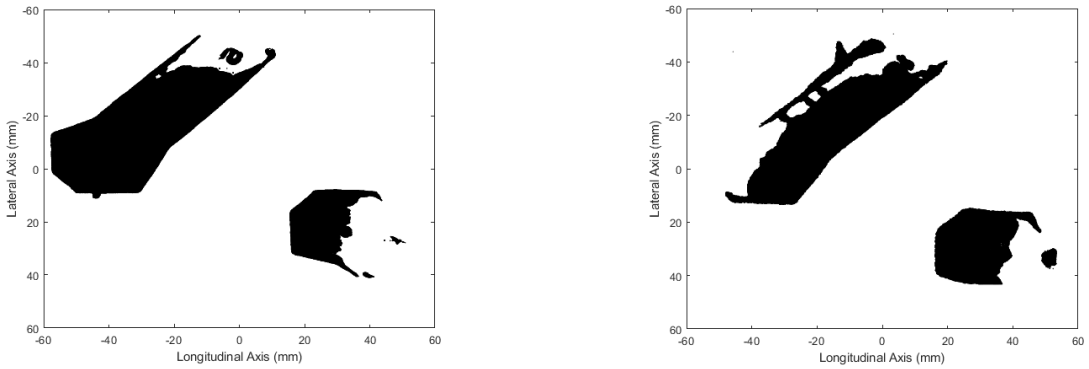

(a) **(b)**

Figure 6.12: Contact patch footprint of agricultural tyre vertically loaded onto a (a) Flat bed and (b) Drum

6.5 Strain gauge trends

Inner surface strain of the tyre is sensitive to changes in tyre operating conditions as was seen from literature. Many of these studies performed on static passenger car tyres. In this section, the inner surface strain of a rolling agricultural tyre will be presented during vertical loading as well as loading at varied slip angles. As the theoretical strain could not be approximated analytically, the strain gauges were used to compare to the results from T2Cam. The higher sampling rate allows for the full strain distribution to be shown. The inner surface of the tyre included three strain gauges namely a longitudinal quarter bridge, a half bridge and a lateral quarter bridge as displayed in Figure 6.13. During testing, the half bridge began debonding which caused its results to be noisy and these were discarded from the study, The strain trends will therefore only be shown for the longitudinal and lateral quarter bridge strain gauge results.

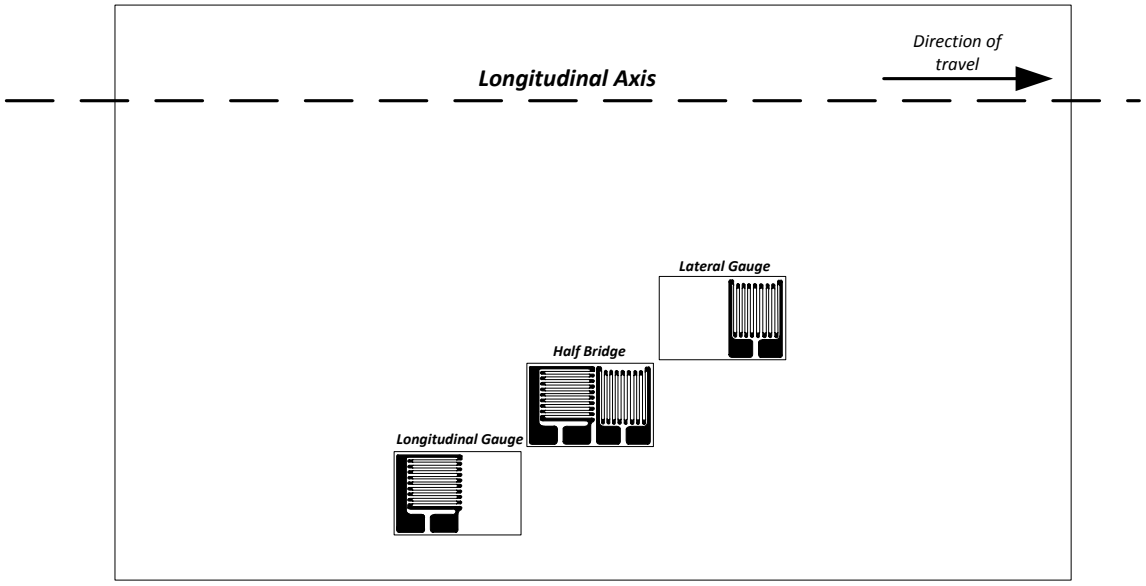

Figure 6.13: Layout and configurations of strain gauges placed within the contact patch of agricultural tyre

6.5.1 Vertical Loading

The test tyre's inner surface strain was measured with increase in load while rolling. The test began with the tyre, set at 0° slip angle, and drum initially stationary. The drum was first brought to steady state speed before the tyre was incrementally loaded onto the drum. The test setup did not have a tuned velocity control thus as the drum was loaded, the velocity inherently decreased. The load was increased until the drum could no longer handle additional load and the test was ended. No speed dependency tests were performed and tests were all done at the same initial speed of 5km/h.

The full strain distribution measured by the strain gauges, with increase in load, is shown in Figure 6.14. The longitudinal strain is shown in Figure 6.14 and the lateral strain is shown in Figure 6.15. Similar to the longitudinal strain trends seen by Morinaga et al. (2006), a tension peak occurs at the centre of the contact patch ($\approx 150°$) and two compression peaks as the gauge enters and leaves the contact patch ($\approx 130°$ and $180°$). Changes due to load can be noted by the increase in these tension and compression peaks, while the areas outside the contact patch remain fairly unaffected.

The location of the maximum tension peak occuring at $\approx 150°$ is seen to shift to the left with increase in load, as seen in Figure 6.14. The black line in Figure 6.14(b) goes through the maximum tension value at the lowest load and shows the shift of maximum tension peaks with increase in load. This can be useful in determining vertical load from strain measurements given that other factors do not also cause this same effect.

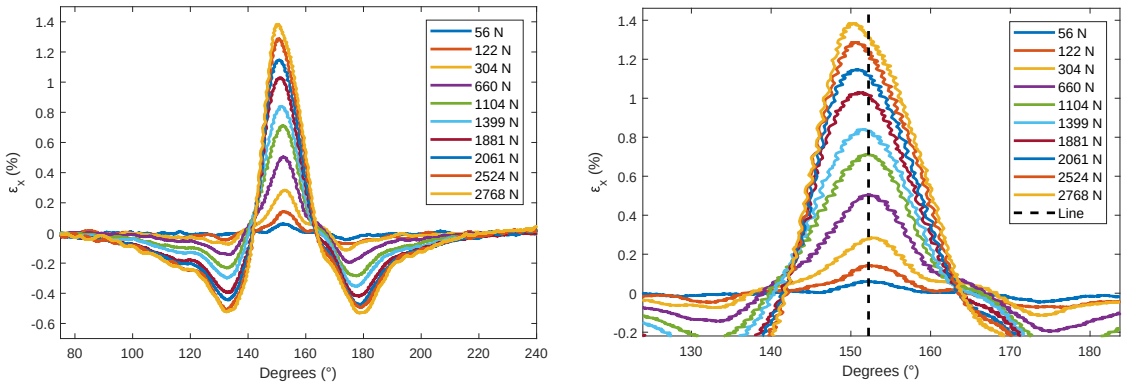

(a) **(b)**

Figure 6.14: Longitudinal strain gauge results with increase in vertical load (2.0 Bar, 5km/h) with the results given as (a) Full Distribution (b) Zoomed in section

The longitudinal strain showed a symmetrical strain distribution for purely vertical loading, contrary to the lateral strain. The lateral strain distribution at different increasing vertical loads is shown in Figure 6.15(a). The distribution changes in shape considerably between low and high loads and is therefore split up in Figure 6.15(b) and Figure 6.15(c). At lower loads (Figure 6.15 (b)), the lateral strain distribution is similar to the trends seen by Morinaga et al. (2006) with a difference seen in the asymmetry of the two tension peaks. At higher loads (Figure 6.15 (c)), a third tension peak is introduced to the strain distribution at the centre of the contact patch. Asides from increases in tension and compression peak

values, the trends of the lateral strain changes at increasing vertical loads where the centre of the contact patch changes from experiencing compression to tension. This is due to the increased load causing more contact between the drum and tyre and another tread block making contact with the drum. Above in Figure 6.14, the longitudinal results are not affected by the increased tread to drum contact and little change is seen between the trends at lower and higher loads.

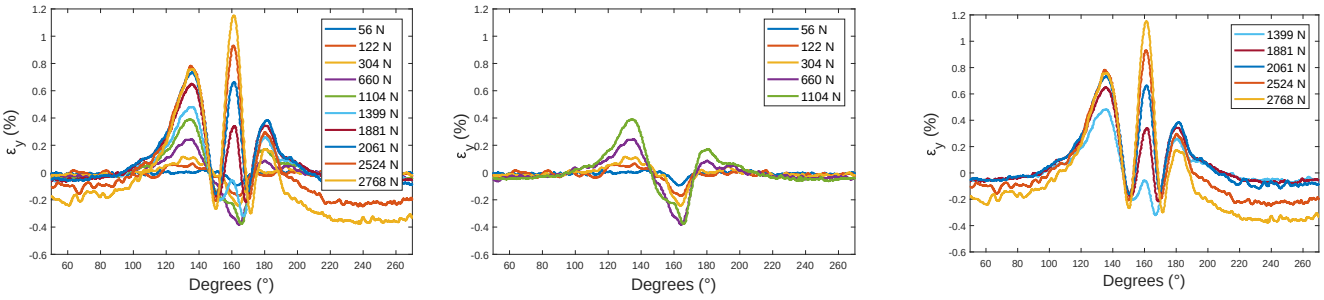

(a) **(b)** **(c)**

Figure 6.15: Lateral strain gauge results with increase in vertical load with (a) all loads and (b), (c) are the results split up between low loads and high loads

In the interest of developing a smart tyre, it is important to understand sensors sensitivities to changes in tyre working conditions. From literature it was seen that passenger car tyres have similar strain distribution trends. The strain distribution is governed by the motion of the tyre as it moves through the contact patch therefore a similar trend should be seen by an agricultural tyre. Peak tension and compression values have the most sensitivity to changes in tyre operating conditions, these points of interest are indicated in Figure 6.16.

The strain distribution used to demonstrate this is the test tyre at straight line conditions. The lateral strain showed a change in strain distribution at higher loads, the lateral strain is differentiated between low load and high load in Figure 6.16B and 6.16C respectively. The effect where the centre of the contact patch changes from compression to tension lateral strain was seen with increase in load and change in slip angle. The two compression peaks for Figure 6.16C were seen to be equivalent and therefore were not individually measured. It is expected that results will still be comparable to this distribution at varied slip angles. These points will be used to find the level of sensitivity and relation to operating conditions at different test results.

The longitudinal (Figure 6.14) and lateral (Figure 6.15) inner surface strain at the key points shown in Figure 6.16 are used to show strain sensitivity to change in vertical load. The longitudinal and lateral strain relationship to load is seen in Figure 6.17(a) and (b) respectively.

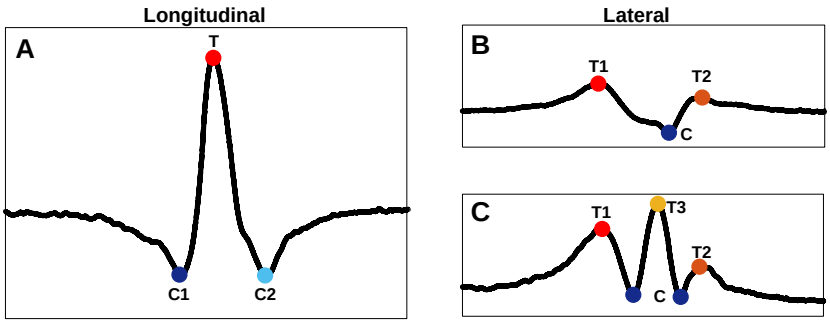

Figure 6.16: Key points for measurement for the inner surface strain distribution in the (A) longitudinal direction and the lateral direction at (B) low loads and (C) larger loads

The longitudinal strain has a linear relationship with vertical load for both tension and compression peaks (Figure 6.17 (a)). The two compression peaks (C1 and C2) can be seen as equivalent for a purely vertical loading. The coefficient of determination (R^2) is above 0.97 for all the key points of measurement for the longitudinal strain. The lateral strain experienced a less linear relationship to increase in vertical load. The lateral strain underwent a change in distribution surpass 1250N which introduced a third tension peak (T3), T3 had the most linear relationship with increase in vertical load. A fairly linear relationship was seen for both T1 and T2 prior to the development of T3, thereafter the relationship can no longer be described as linear. The load at which T3 appears at is a low load in comparison to the loads expected during normal working conditions (LI is 9810N at 2.0 Bar). Therefore, the linear relationship between T3 and load can be useful when measuring sensitivity to vertical load on lateral strain.

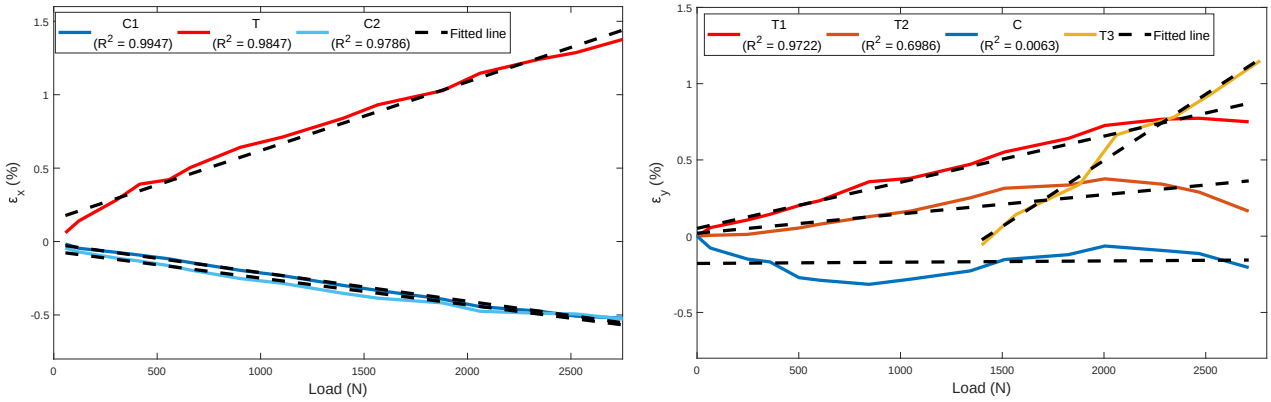

(a) **(b)**

Figure 6.17: Maximum (a) Longitudinal and (b) Lateral tension and compression peak strains during vertical loading at 2.0 Bar

Inflation pressure also has an effect on tyre deformation. A higher inflation pressure results in a stiffer tyre and less tyre deformation and vice versa at lower inflation pressures. The effect of inflation pressure on longitudinal and lateral strain can be seen in Figure 6.18 at a low and high load of 700N and 1400N. A lower inflation pressure is seen to produce larger compression and tension peak values for the longitudinal strain in Figure 6.18(a). The same is seen in the lateral strain, although the strain at 1.6 Bar experiences a larger tension peak value for the newly induced tension peak due to increase in tread contact.

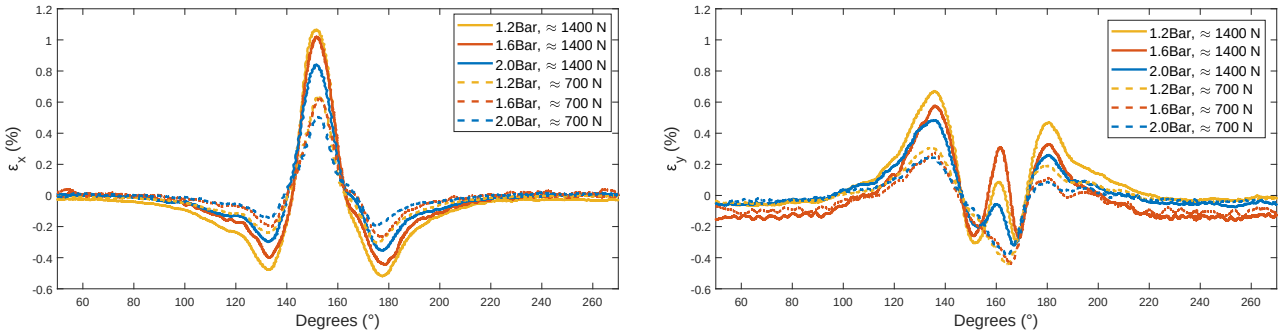

(a) **(b)**

Figure 6.18: (a) Longitudinal and (b) Lateral results at a low and high load at test pressures of 1.2, 1.6 and 2.0 Bar

6.5.2 Varied Slip angle

The tyre was tested at five slip angles namely 3.22°, 2.15°, 1.16°, -1.67° and -2.68°. The test setup had capabilities up to ± 15° however for this study less evasive cornering conditions were tested. Each slip angle was tested at an initial speed of 5km/h and increasing vertical loads. The nature of the testing did not allow for consistent loading. Therefore, tests were compared at the closest load match. The varied slip angles will be compared at a vertical load of 700N, 1300N and 1600N.

The tested slip angles at a vertical load of ≈ 1600N is shown in Figure 6.19. The longitudinal strain (Figure 6.19(a)) shows little change at varied slip angles, with the largest change occurring at around 160°, the same region where the third tension peak is developed as seen in the lateral strain distribution (Figure 6.19(b)). The lateral strain is greatly sensitive to change in slip angle while the longitudinal strain remained fairly constant at varied slip angles.

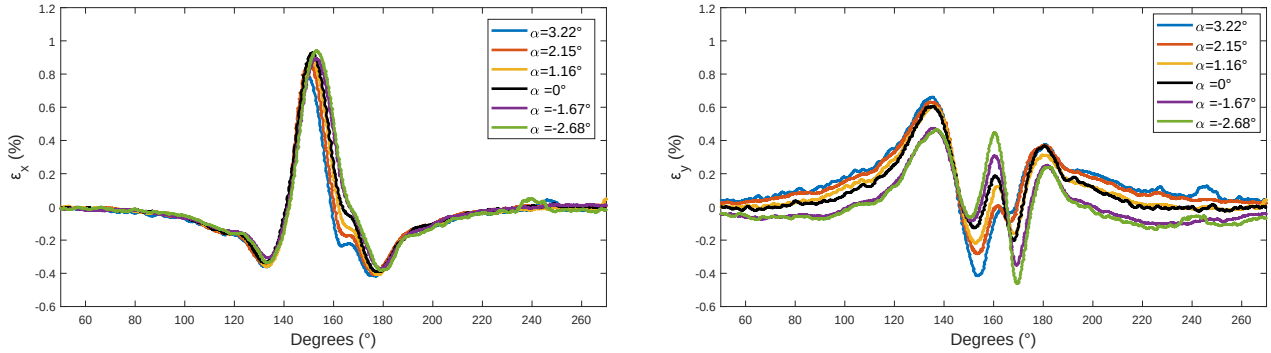

(a) **(b)**

Figure 6.19: (a) Longitudinal and (b) Lateral strain distribution for varied slip angles at a vertical load ≈ 1600N

The key measurement points as previously shown in Figure 6.16 is used to show the relationship between strain and slip angle. The longitudinal and lateral strain peaks at varied slip angles is shown in Figure 6.20 (a) and (b) respectively. The T3 values are not shown for this section as this peak is not always prominent at all slip angles. The two compression

peaks for the lateral strain are the most sensitive to change in slip angle and this relationship is seen to be linear in Figure 6.20 (b). The two tension peaks for the lateral strain also show a linear relationship, yet not as sensitive as the compression peaks. The longitudinal strain as seen in Figure 6.20 (a) shows little sensitivity to change in slip angle.

The two lateral compression peaks in Figure 6.20 (b) appeared to be inversely proportional, however, this differed at lower loads. The lateral force may have saturated at higher slip angles causing this. Unfortunately, the lateral force was not measured during testing to confirm this. Similar results are seen in Figure 6.21 at a slightly lower load of ≈ 1300N before loss of adhesion.

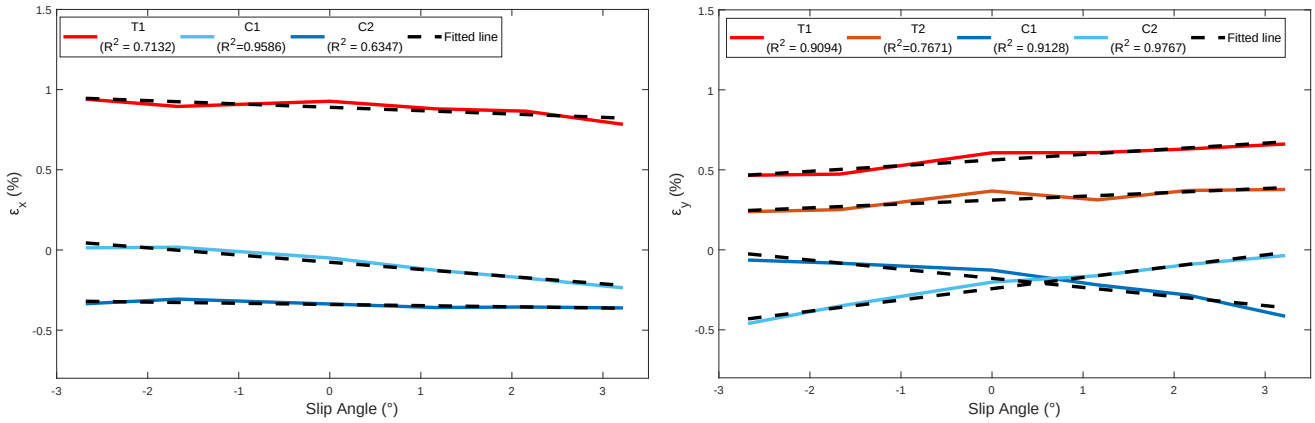

(a) **(b)**

Figure 6.20: Maximum (a) Longitudinal and (b) Lateral tension and compression peak strain measurements at different slip angles (≈ 1600N)

The strain at varied slip angles at a lower vertical load of 1300N is shown in Figure 6.21. The longitudinal strain in Figure 6.21(a), as seen previously, shows very little sensitivity to change in slip angle. The offset lateral strain outside of the contact patch is affected by change in slip angle in Figure 6.21(b). The peak values at T1 and T2 show small variations to change in slip angle for the lateral strain with the largest variation at the centre of the contact patch. The value of T3 increases moving from positive to negative slip angle and is the same for C1. The sensitivity of lateral strain peaks to change in slip angle is shown in Figure 6.23.

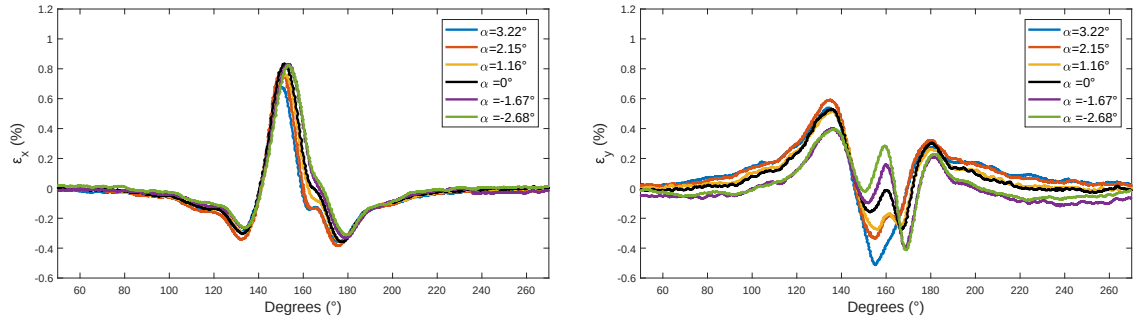

(a) **(b)**

Figure 6.21: (a) Longitudinal and (b) Lateral strain distribution for varied slip angles at a vertical load ≈ 1300N

A third comparison at a vertical load of ≈ 700N is shown in Figure 6.22. Here it can be seen that T3 only develops at negative slip angles while the positive slip angles remain with two tension peaks. The longitudinal strain is again seen to show little sensitivity to change in slip angle. The lateral strain is sensitive to lateral loading, its sensitivity at a vertical load of 700N and 1300N to slip angle is shown in Figure 6.23.

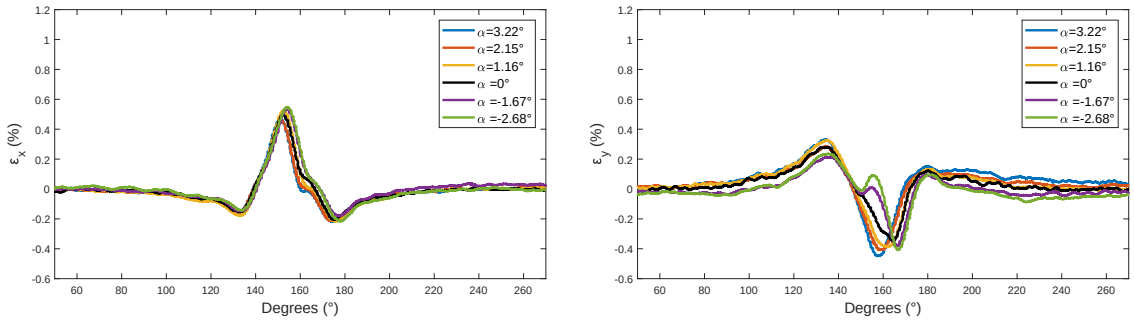

(a) **(b)**

Figure 6.22: (a) Longitudinal and (b) Lateral strain distribution for varied slip angles at a vertical load ≈ 700N

The two tension peaks, T1 and T2, for the two vertical loads in Figure 6.23 show equivalent changes, with both being fairly insensitive to change in slip angle. When comparing C1 and C2 between the two vertical loads, it is noted that C1 has the most linear relationship with change in slip angle.

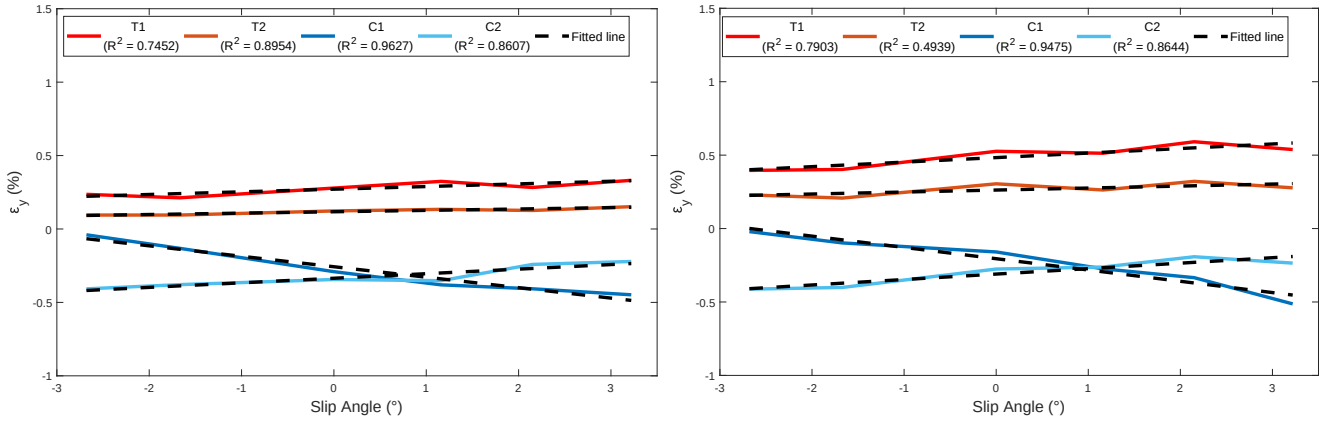

(a) **(b)**

Figure 6.23: Maximum lateral tension and compression peak strains at different slip angles at vertical loads of (a) ≈ 700N (b) ≈ 1300N

The change in slip angle has an evident effect on the lateral strain results with small effects on the longitudinal strain. In particular, the lateral strain compression peaks will be useful for lateral force estimation. The two lateral compression peaks at the three vertical loads is shown together in Figure 6.24. It can be seen that C2 is more dependent on slip angle than on vertical load. C1 in particular is fairly insensitive to vertical loading while sensitive to lateral loading. The compression peaks of the lateral strain distribution should thus be used for lateral force estimation as they are the most sensitive variable to lateral loading.

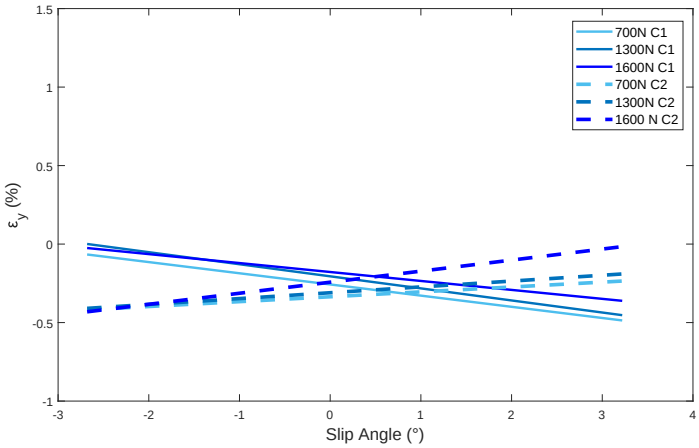

Figure 6.24: Compression peak values for lateral strain distribution at varied slip angles and vertical loads

6.5.3 Discussion of strain gauge results

Tyre strain measurement has been focused on point measurement via the inner surface of passenger car tyres in literature. While little work as been done on strain measurement of agricultural tyres, it was seen that there are similarities between the two different tyre structures. The common longitudinal strain distribution seen for passenger car tyres under purely vertical load was seen to be a tension peak at the centre of the contact patch and two symmetric compression peaks at the beginning and end of the contact patch. This distribution is due to the motion of the tyre through the contact patch, this is a common phenomena for agricultural tyres. It is expected that any deviations from common strain distributions, would be due to the large lugs present on agricultural tyres. The presence of a third tension peak for the lateral strain was not commonly seen in literature. For instances where a third tension peak was developed in literature, the magnitude of the peak would not be of a large magnitude.

For point measurement, passenger car tyre studies show similar general strain trends regardless of the different locations of measurement. Within this study, Variations in magnitudes and symmetry is seen to be due to placement location as well as tyre operating conditions such as inflation pressure, vertical load and slip angle.

6.6 Differences in full-field to point measurements

Pairing several strain gauges placed on the inner surface of the tyre can give information of slip angle and tyre camber. Full-field strain measurement can be incredibly useful in this aspect as well as measurement of the entire region. The in-tyre camera system, T2Cam, can be compared to strain gauge measurement by tracking a point from start to end of the contact patch acting which will act as a point strain measurement. This comparison was done for straight-line rolling at 2.0 Bar.

As discussed, the strain gauges and T2Cam could not be compared at the same location/time sequence. The region where the strain gauges are applied is hidden with silicon

and leading wires, which have different properties to the rubber and inevitably will result in a large amount of missing points. The tyre has a repeating pattern with every lug; therefore, the full-field strain measurement can be measured at a later lug within the same revolution. T2Cam images used to compare with strain gauges were chosen at a region where the most images were taken for the best sampling rate.

The point strain measurement from T2Cam and the strain gauge measurements comparison is shown in Figure 6.25. The comparison is shown at multiple loads. The temperamental nature of the camera triggering did not allow for a constant sampling rate and this can be seen by varying sampling rate. The best comparison, in terms of sampling rate, can be seen in the third plot at 2524N which validates both measurements.

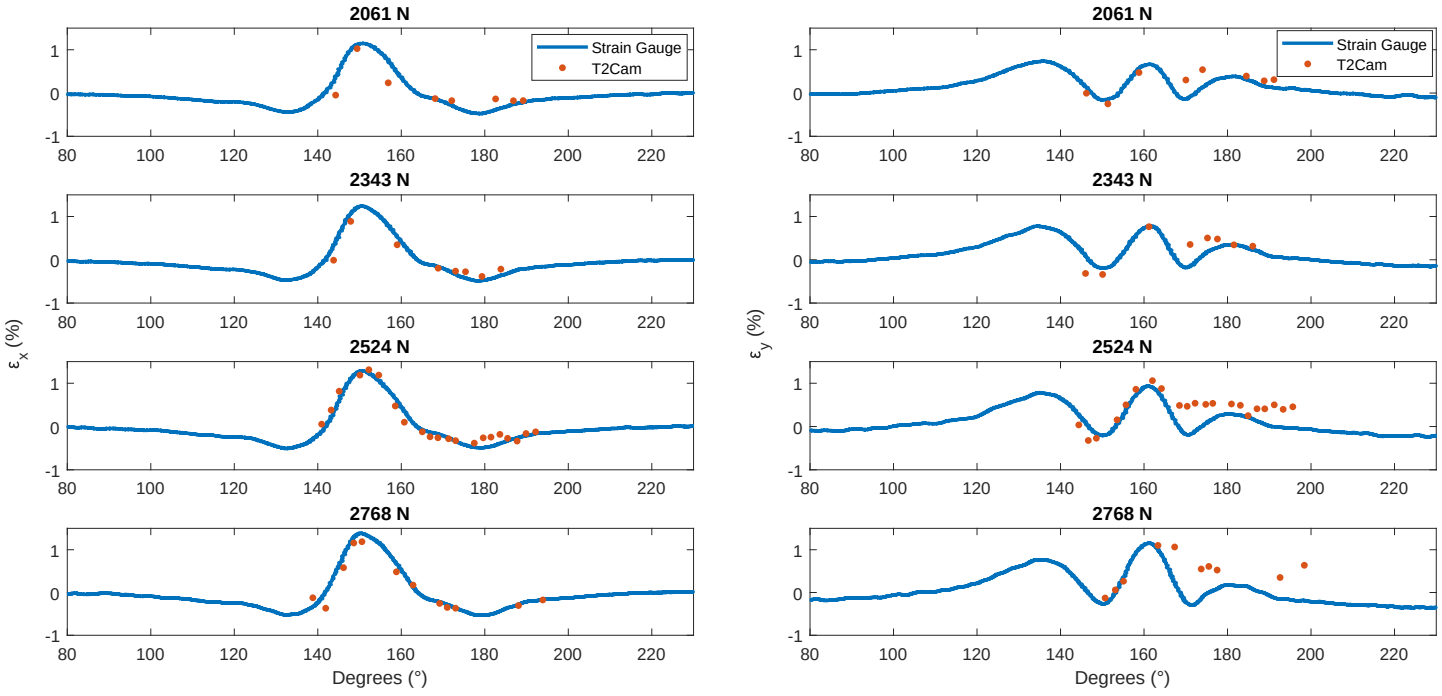

(a) **(b)**

Figure 6.25: Comparison of (a) Longitudinal and (b) Lateral strain from full-field and point measurement at three vertical loads (2.0 bar, 5km/h)

The closest to ideal sampling rate provides a clear comparison between full-field camera measurement and point strain gauge measurement. The longitudinal strain measurements correlate well and can be further improved with improvements to the current sampling rate. However, the lateral results only show good correlation up to the second compression peak. The full-field measurements were seen to be very noisy towards the end of the contact patch and the loss in correlation towards the end may be due to this.

Figure 6.25 illustrates the capability of T2Cam to measure strain dynamically. However, these results illustrate the necessary improvements which need to be made to further the measurement possibilities. The current sampling rate is poor and does not produce com-

parable results. With the compression peaks shown to be greatly sensitive to parameter changes in the strain gauges, it is important for T2Cam measurement analysis to capture this valuable information. T2Cam measurement includes point tracking over several images. Each image should individually show change in tyre operating conditions and multiple images showing the change over the full strain distribution. For vertical load and slip angle, T2Cams sensitivity to change in these parameters will be shown with individual images. This will be a more effective measure of full-field strains sensitivity to parameter changes. This is, however, for a single image and thus a single instance while the above comparison done in Figure 6.25 is for a complete motion through the contact patch with a strain distribution over several instances.

6.7 Effect of lug contact pattern

With a large lug tyre, the contact between road and tyre is constantly changing even in constant tyre operating conditions. As the tyre rolls, it makes contact with the road with different quantities of lugs and different orientations of these. Contact patterns are dependent on time and this changing contact is illustrated in Figure 6.26. A change between one lug contact to two lugs contact results in a substantially different individual full-field strain measurement. Instantaneous comparisons of contact patch strain can only be done with images of the same contact region, which often is not captured repetitively throughout each revolution within a test.

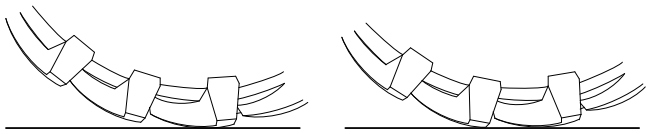

Figure 6.26: Changing contact between road and agricultural tyre

An improved sampling rate is required to capture the constantly changing measured area. With a smooth treaded tyre, a single image can suffice for an entire contact patch strain measurement. The strain gauge is required to travel through the contact patch for a complete measurement while an entire strain distribution can be measured by a single image pair from T2Cam. With all operating conditions constant, the strain distribution will remain constant inside a passenger car tyre due to the fairly smooth tread pattern. This makes the contact patch independent of what angle the tyre is rotated to. A large lug tyre has extremely complicated strain patterns with the trends changing with every change in rotation. Therefore, in a smooth treaded tyre the strain caused by tyre structure is kept constant and the only variation in strain is due to change in other tyre operating conditions. T2Cam's low sampling rate is unfavourable for an agricultural tyre however, is more than sufficient for a tyre without large lugs, such as a passenger tyre, thus removing the complexity of largely varying strain trends.

The agricultural tyre has 17 lugs, therefore strain trends are repeated 17 times within one revolution with one full cycle occurring every $\approx 21^{\circ}$. This gave multiple opportunities for comparison, one region in particular had a suitable sampling rate as seen in Figure 6.6 while the other 16 lug regions did not have sufficient sampling frequency for comparable

results. One full cycle is shown in Figure 6.27 and Figure 6.28 where each plot is the longitudinal/lateral strain at a discrete time instance. Figure 6.27 and 6.28 illustrates how the contact patch strain field changes as it is rotated while keeping all operating conditions constant. A tread pattern is overlaid to illustrate this movement of a tread pattern through the contact patch. It must be noted that this overlay is not the exact contact pattern, this is added to give an indication of where the lugs are situated under the inner surface.

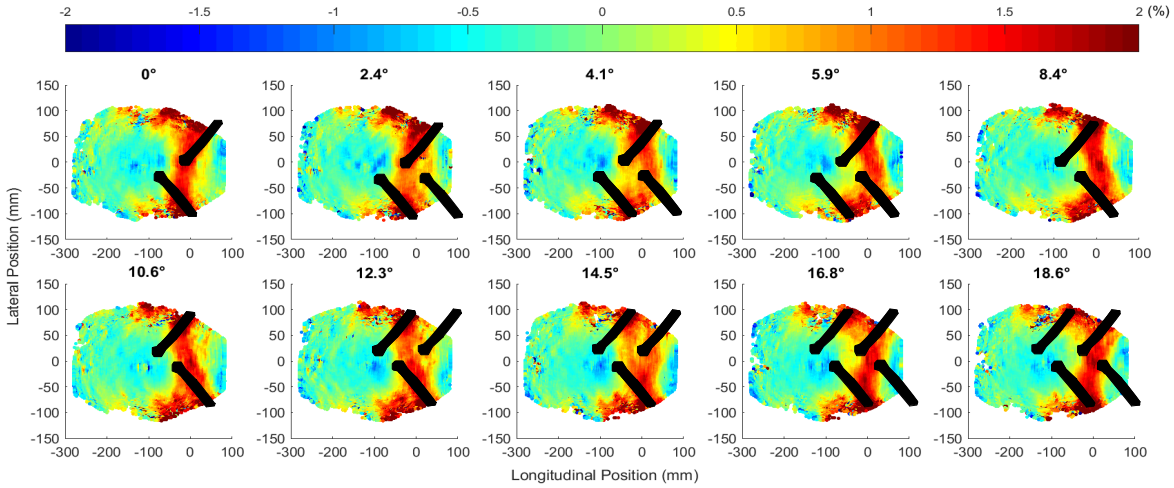

Figure 6.27: Longitudinal strain of discrete moments as tread block travels through contact patch

The longitudinal strain plots in Figure 6.27 show the movement of lugs through the contact patch and how the strain distribution changes with every change in rotation. The lateral strain in Figure 6.28 does not show this as clearly, however, tension strain concentrations can be seen around the entering lugs. The plots shown in Figure 6.27 and 6.28 demonstrate that the location of measurement relative to the lug is important for sensitivity as the largest strains are experienced around the lug. It should be noted that strain measurements can drastically change by even the smallest of change in measurement location.

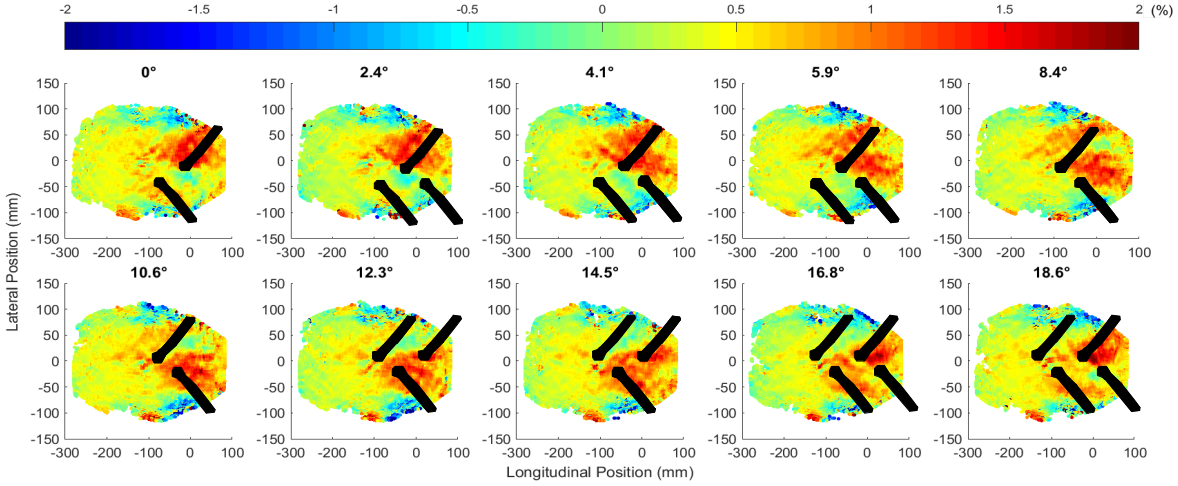

Figure 6.28: Lateral strain of discrete moments as tread block travels through contact patch

The variation in strain as the tyre rotates is shown for a strain distribution along the length of the contact patch plot in Figure 6.27. A waterfall plot of the longitudinal strain along a lateral position of 20mm demonstrates the movement of the lugs moving through the contact patch in Figure 6.29 as well as additional instances. The longitudinal results showed this effect more clearly than the lateral results. The entry of a new lug can be seen with repeating patterns. All other parameters were kept constant during the capturing of the images in Figure 6.29. It can be seen that different angular regions experienced different sensitivities and different magnitudes will be experienced at different measurement locations. Certain point locations are seen to be more sensitive to vertical load and highlights the importance of point measurement location especially in an agricultural tyre.

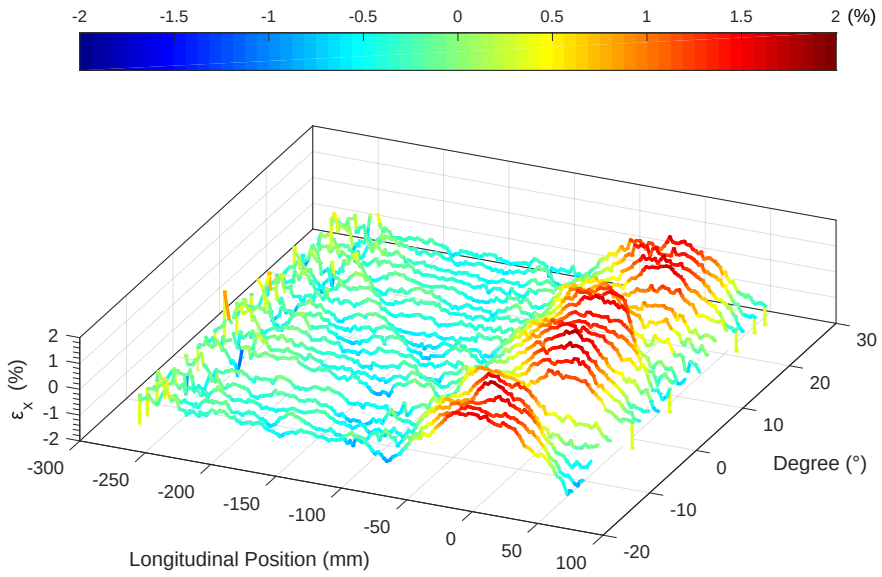

Figure 6.29: Waterfall plot of longitudinal strain showing movement of tread block through contact patch

Parameter changes resulting in phase shifts and magnitude increases will be coupled with the effect of tyre structure which will add difficulty for parameter estimation should not the same region be used per comparison.

6.8 T2Cam load sensitivity

As stated previously, it is difficult to aptly correlate T2Cam strain measurement with the strain gauges with a single image with each image hosting varying strain patterns. There were few single regions which were successfully captured for all rotations of a single test with increase in load. Instead of finding the maximum tension and compression for a single point as it moves through the contact patch using multiple consecutive images, the strain is determined for the same region for each revolution. This is representative of the overall effect on strain with increase in load.

A single region, which was captured over multiple revolutions, is used to show the strain distribution taken along the centreline with increase in vertical load in Figure 6.30. A gen-

eral distribution is seen with an increase in vertical load causing an increase at the multiple peaks. The dotted line in Figure 6.30(a) indicates that there is no phase shift of the maximum tension peak as the vertical load is increased. The increase in peak values can be used for vertical load estimation.

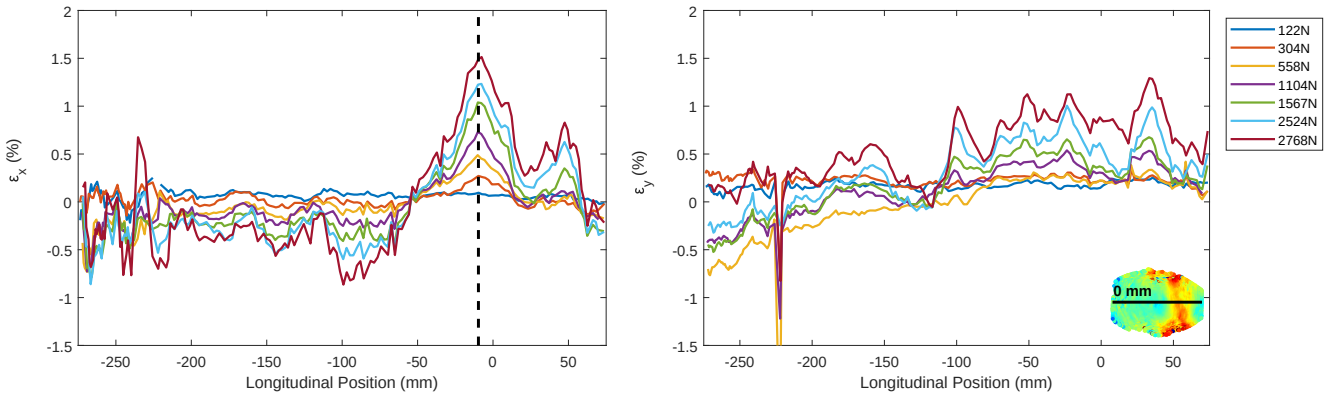

Figure 6.30: Load sensitivity: Longitudinal and lateral strain along the centreline with increase in vertical load

The maximum tension and compression values for the captured region in Figure 6.30 are plotted against increase in vertical load in Figure 6.31. This cannot directly be compared to the tension and compression peaks, and their relationship to tyre operating conditions, as measured by the strain gauges. The maximum peak values plotted in Figure 6.31 may not necessarily be the maximum strain values should a point measurement be taken through the whole contact patch, this method merely uses the increase of maximum strain values as a measure of increase in vertical load. For this, the measurements left of -150mm along the longitudinal axis is ignored due to measurement noise. The dip occurring in Figure 6.30(b) at -220mm was noted to be due to speckle of dirt appearing over that region during the duration of the vertical loading test. It is important that this analysis is only done for strain measurements from the same region. A region may have larger strain profiles due to the tyre structure and therefore, could result in peaks due to the tyre structure and not load or other condition changes.

Vertical load and longitudinal strain had a linear relationship with a $R^2 > 0.97$ as measured by strain gauges in Figure 6.17. Similarly, a linear relationship ($R^2 \approx 0.96$) is seen between vertical load and longitudinal strain as measured by a single region with T2Cam. The lateral strain as measured by the strain gauges was found to have two tension peaks, both differing in magnitude, and a third tension peak which emerged at higher vertical loading. For the strain measured by T2Cam, there are several tension peaks in Figure 6.30 which are not necessarily comparable to the differing tension peaks as measured by the strain gauges. Thus, only the overall maximum tension and compression is plotted for the lateral strain measured by T2Cam. This is considerably different to the comparison done for the strain gauges however is representative of the influence of vertical load on lateral strain measurement.

It is also important to note that a linear relationship with vertical load is seen by analysis of a single image pair and thus does not require a full travel through the contact patch

before changes in strain distribution can be seen. The lateral strain in Figure 6.31, however, does not show the noticeable increase in contact between tyre and drum as seen by the development of T3 in the strain gauge's lateral strain. While a single image pair analysis does demonstrate a linear relationship with increase in vertical load, more information can be gathered with a full strain distribution analysis. Improvement of the current sampling rate of T2Cam will enable this and further the capabilities of the camera system.

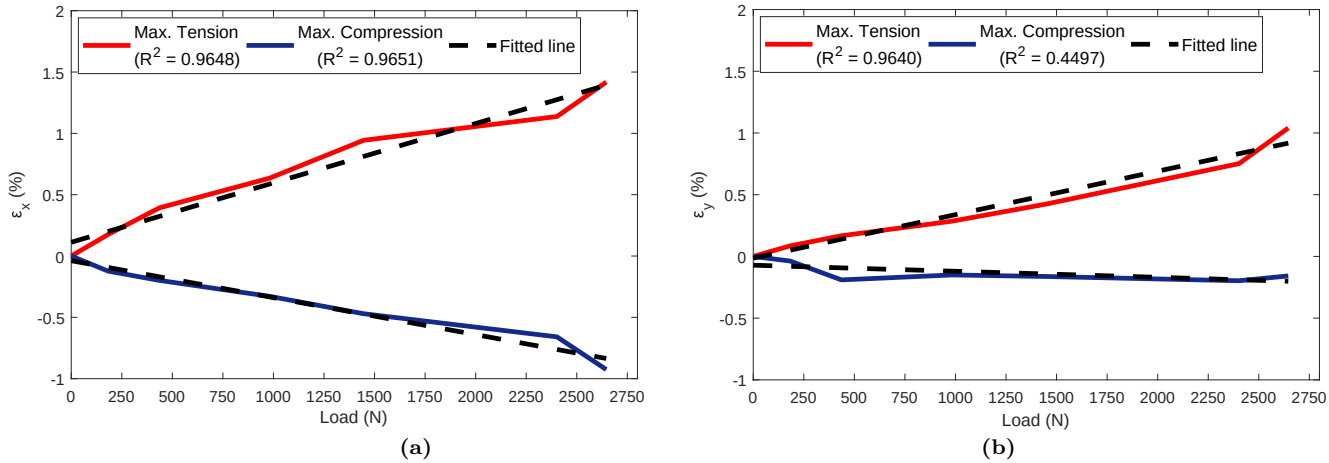

Figure 6.31: Maximum (a) Longitudinal and (b) Lateral tension and compression peak strains with increase in vertical load (2.0 Bar, 5km/h)

The location of the lugs in the contact patch influences the strain pattern asides from the other contributing factors such as inflation pressure, vertical load and slip angle. Different magnitudes and trends are found at different points of measurement. To demonstrate this, a second analysis is done for the same image but along the same lateral position as the longitudinal strain gauge, the longitudinal and lateral strain along this length at increasing vertical load is given in Figure 6.32. Again, a dotted line is included for the longitudinal strain to highlight that the maximum tension peaks occur at the same longitudinal position. The strain distribution as measured by the strain gauges showed very distinct regions of tension and compression, the maximum strain magnitudes for this region are plotted in Figure 6.33 with vertical load to find the relationship between the two.

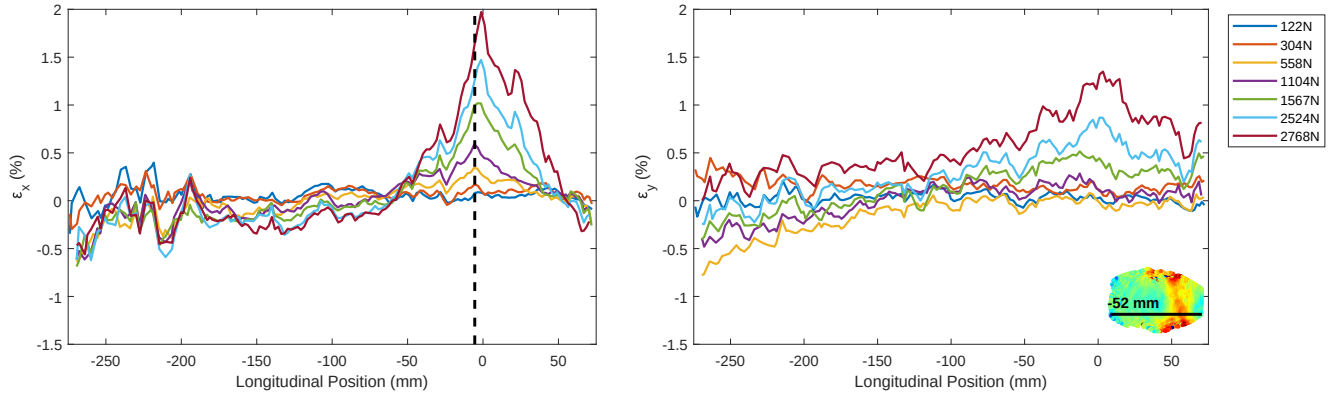

Figure 6.32: Load sensitivity: Longitudinal and lateral strain along the centreline with increase in load (second region)

It was clear from the strain gauges that an increase in load caused a phase shift which could be useful for predicting vertical load from strain measurement, this effect was not seen from T2Cam. The trends between different lateral locations did not differ severely while the magnitude was a noticeable difference.

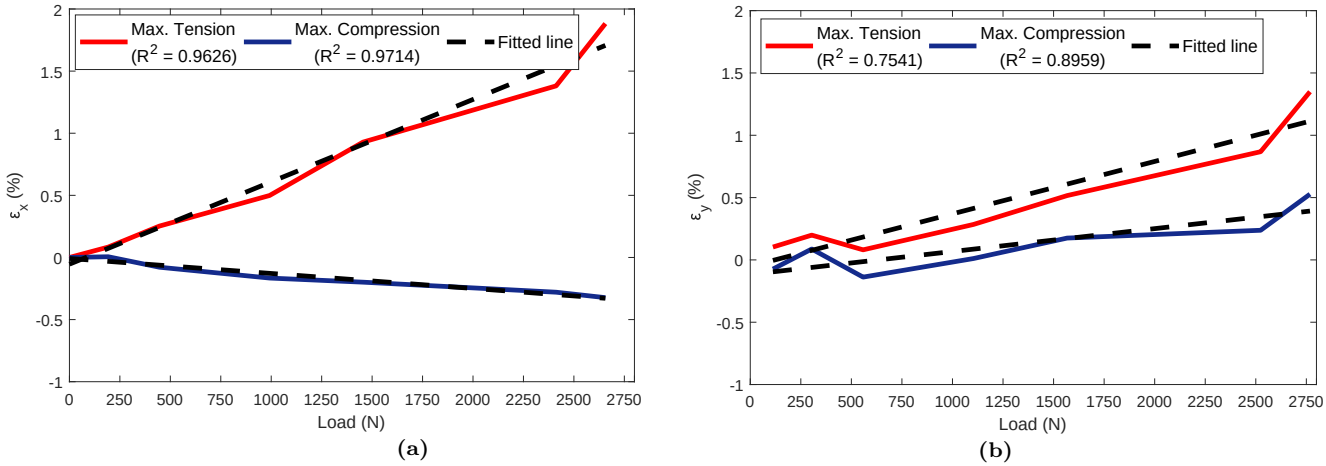

Figure 6.33: Maximum (a) Longitudinal and (b) Lateral tension and compression peak strains with increase in vertical load (2.0 Bar, 5km/h)

The region used for load comparison can be seen to have an effect on trends with increase in load. The tension trends remain the same between the two regions whereas the compression shows a different relationship with increase in load. Each region has a different, while not greatly, effect from change in load. The change in maximum strain magnitudes for a full distribution over several images will need to be found in future work.

6.9 Comparison of different slip angles

Cornering conditions were seen to show little effect on longitudinal strain. Larger effects were seen in the lateral strain from strain gauge testing. For full-field strain analysis, the longitudinal and lateral strain is measured along three lateral positions. A single image pair is used to show T2Cam's full-field strain sensitivity to change in slip angle. The measurements along the three positions are shown in Figure 6.34. Strain concentrations appear close to the edges of the contact patch. Therefore, differences between centreline and edge measurements is expected. The edge measurement was taken at the same lateral position as the Longitudinal Gauge as seen in Figure 6.13 and the reflection of it about the centreline. The positive and negative positions have different lug patterns thus both were plotted to find comparable changes. The top plot in Figure 6.34 was the least affected by noise and this was used to show the relationship between slip angle and maximum strain magnitudes. The other two positions were too noisy for analysis. The cause of noise is most likely due to a combination of noise present at the edges and small speckles of dirt present on the camera lens in those regions. As shown by the waterfall plot in Figure 6.29, each region has different sensitivities. The regions which were captured during all slip angle tests at the correct load were limited and the region which was available for analysis may have been a region of low sensitivity to change in slip angle. Improvements of the camera system will allow more regions to be captured for further comparison.

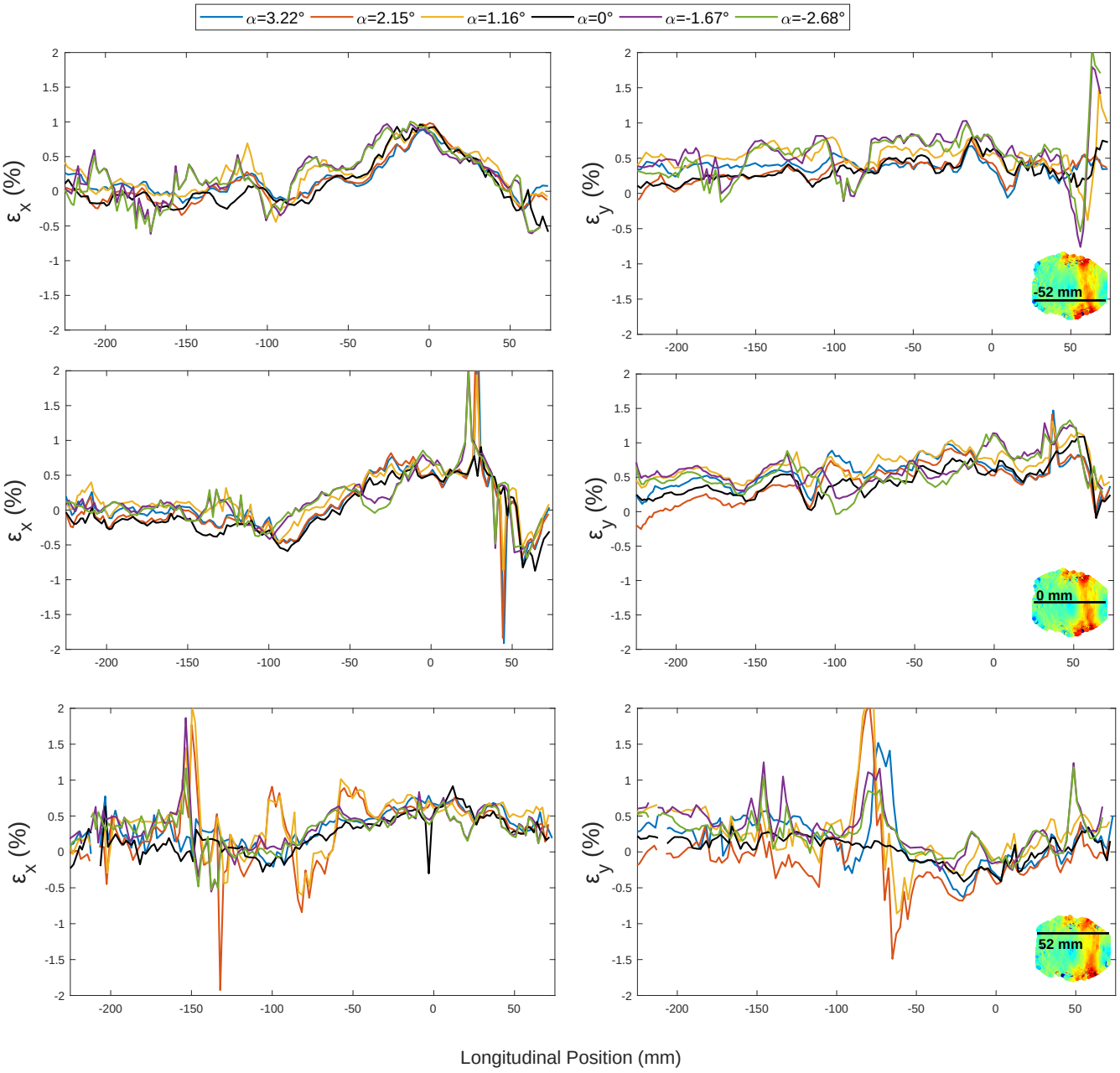

Figure 6.34: Slip angle sensitivity: Longitudinal and lateral strain along three lateral positions with change in slip angle (1600N, 2.0 Bar, 5km/h)

The strain experienced at different slip angles changes slightly in shape with small differences occurring at the peak values. The most change is seen between negative and positive slip angle as there is a horizontal offset. The maximum tension and compression magnitudes at the tested slip angles is shown in Figure 6.35 for the negative lateral position. Both longitudinal and lateral strain is shown. The tension shows a general increase with positive increase in slip angle however, a negligible change in comparison to load sensitivities as was seen in Figure 6.33. The compression peaks show a noticeable sensitivity, with the lateral compression peaks being slightly noisier. It can be noted that the compression peak is more sensitive to change in slip angle. A fitted line for the longitudinal strain values in Figure

6.35 is included and thus shows that the compression peak values are more sensitive to change in slip angle.

The lateral strain was seen to noticeable change with slip angle in the strain gauges however, for full-field measurement it proved to be a less reliable measurement of slip angle. Yunta et al. (2019) found that the tension for both longitudinal and lateral strain remained constant at varying low slip angles. The compression peak for the longitudinal strain showed the most influence with an increase in magnitude with increase in positive slip angle. This effect is rather small in comparison to that of the vertical loading.

Detecting loss of adhesion from strain measurements will be highly beneficial for vehicle stability systems. Tyre saturation typically occurs at slip angles above 4°, beyond the range which was tested. Finding a relationship between lateral force and strain could provide slip angle measurement given the vertical load, which can be measured from the linear relationship with longitudinal strain. This warrants further testing at larger slip angles in future works.

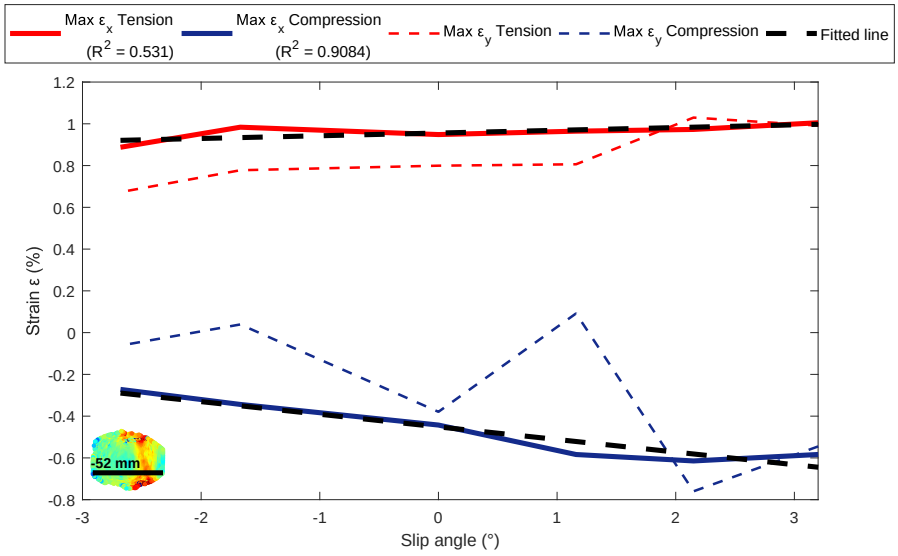

Figure 6.35: Maximum Longitudinal and Lateral tension and compression peak strains with change in slip angle (1600N, 2.0 Bar, 5km/h)

T2Cam strain measurement has shown to be sensitive to tested parameter changes. The system has the benefit of providing a clearer picture of the entire contact patch which may highlight more interesting phenomena than discrete point measurements. With an improved sampling rate, the efficacy of full-field measurement to produce a full strain distribution will be achievable.

6.10 Discussion of results

System limitations and testing methods hindered full strain distribution measurement. With these unfortunate effects, propitious results were fortunately seen. Longitudinal and lateral

strain were both sensitive to vertical load with longitudinal strain showing a linear correlation of $R^2 > 0.97$. The vertical load was seen to have the greatest effect on the contact patch strain. Slip angle caused a small effect on the maximum strain however, the results from the strain gauges were promising and interesting phenomena is expected when testing at large slip angles in future works.

The lugs were seen to have an effect on the strain fields and the location of measurement is important for sensitivity for a large lug tyre. The non-homogeneous tread pattern results in a non-homogeneous strain field. Location of point measurement can significantly influence results and therefore selecting placement of strain gauges requires thorough analysis prior.

Camera effects, such as motion blur, are seen to be negligible. When compared, the full-field measurements were in accordance to the strain gauge measurements. Avenues for future work exist when correlating lateral force and tyre strain such that, when the tyre begins to lose grip and therefore, a decrease in deformation, strain can be used to indicate this.

The use of strain gauges on the inner surface of the tyre has shown that inflation pressure, vertical load and slip angle can be estimated from point strain measurement. Monitoring several point measurements at different locations through the same maneuvers can allow for interesting phenomena to be captured, this is possible with T2Cam. T2Cam has shown to be comparable to strain gauges for purely vertical loading. At cornering conditions, however, useful information cannot be extracted as was for strain gauges. Improvement in the testing and triggering system will thus further the capabilities of T2Cam to allow for slip angle estimation.

Chapter 7

Conclusion and Discussion

The contact patch is the point of contact between the vehicle and the road and the interface where majority of vehicle forces are transferred. Directly measuring this interface has proven difficult when operating under typical driving conditions. Strain measurement, above acceleration and deflection, has been shown to give insightful information of the contact patch and, when analysed, could lead to estimations of tyre states. The contact patch strain, of an agricultural tyre, has been measured via the inside tyre surface using a stereo camera system tuned specifically for an in-tyre application. The tyre was dynamically tested on a drum at varying inflation pressures, vertical loads, and slip angles to find how this affects strain measurements.

The agricultural tyre is a complex tyre structure to predict tyre states. The large lugs of the tyre were seen to have an effect on the rolling tyre where noticeable differences were seen between the agricultural tyre and a passenger tyre. Strain of passenger tyres typically did not experience a third tension peak in the lateral strain distribution, this effect is seen to be due to the large lugs making contact with the test surface as the vertical load was increased. The strain distribution is based on how the tyre deforms its rounded surface when driven over a flat surface therefore results from passenger and agricultural tyres are comparable, where the deviations are due to the lugs.

The tyre is dependent on many conditions and sensitivity to each parameter is seen in full-field and point strain measurement. Strain gauges were placed along an area of high strain in the contact patch based on static testing results. The longitudinal strain measured by the strain gauges showed the most sensitivity to vertical load with a R^2 value above 0.97. The longitudinal strain can be used for vertical force estimation, however, was fairly insensitive to changes in slip angle. The compression peak values for the lateral strain will be useful for lateral force estimation as the strain and slip angle had a relationship with $R^2 > 0.9$. The trends seen by the strain gauges show that point measurements can be used to predict tyre operating conditions and the high sampling rate could allow for future work in real-time. Strain gauges can be applied to tyres for commercial use, however, they are limited in the strains it can measure and can be damaged from high deformations. This can be problematic for agricultural tyres at low inflation pressures. Strain gauges cannot endure prolonged testing and can be easily damaged thus careful choice of application is required to extend the life of the strain gauges.

Strain gauges can measure strain at a high sampling rate, however, provides a contact patch strain distribution only once per revolution. For a large lugged tyre, there are regions of different sensitivities and having a full-field measurement of the contact patch will highlight these differing regions. T2Cam was able to measure strain dynamically at limited low speeds. The system does not have real-time capabilities, however, pairing the system with strain gauges can be incredibly valuable for research. The efficacy of full-field camera measurements to measure strain dynamically has been based on its sensitivity to vertical load and slip angle measured from a single image. Implementing the recommended changes will ensure an improved sampling frequency of T2Cam and thus to measure the full strain distribution from full-field measurements. The potential of measuring strain dynamically has been shown and will allow for further investigations which would yield interesting results.

Chapter 8

Recommendations

The conducted tests were limited to low speeds and loads. Strain measurement has been proven possible at low speeds and thus can be tested at faster speeds and higher loads to excite the tyre. The drum provided a suitable environment for dynamic testing, however, limited the achievable driving conditions. The following changes and additions can be implement:

- Improvements to be made to the triggering system so that images can be captured every $\approx 2^{\circ}$
- Including sand paper on the drum surface will give variation in friction of the test surface for further analysis
- Find optimum region of focus (e.g. along centreline) for 'point' measurement from T2Cam
- Perform dynamic tests on a passenger tyre to investigate strain distribution without the effect of large lugs
- Measure the strain from strain gauges placed on the under tread of the agricultural tyre to note differences between under tread and inner surface strain
- Include outside cameras, especially for an agricultural tyre, to synchronize outside and inside measurement. This can be useful see how the tread blocks engage with the test surface Including braking and traction tests would show interesting results and whether strain measurement is suitable for other driving conditions
- Correlate measurements provided by sensors to tyre dynamics
- The lateral load must be measured during testing at larger slip angles and then correlated to produced strains
- An in-tyre calibration system should be considered such that calibration can happen from within the tyre once T2Cam has been installed to allow for possible disturbances during installation or readjustment of focal length

Such changes are recommended in order to elucidate full-field dynamic strain measurement.

Bibliography

Anghelache, G. and Moisescu, R. (2011). Measuring system for investigation of tri-axial stress distribution across the tyre – road contact patch. Measurement, 44:559–568.

Botha, T. and Els, S. (2014). Rough Terrain Vehicle Side-slip angle measurement using digital image correlation. Proceedings of the 18th International Conference of the ISTVS.

Botha, T., Shyrokau, B., Els, S., and Holweg, E. (2015). Kinematic analysis of a tyre rolling over rough terrain using digital image correlation. Proceedings of the 13th ISTVS European Conference.

Botha, T. R. (2015). Digital Image Correlation : Applications in Vehicle Dynamics.

Braghin, F., Brusarosco, M., Cheli, F., Cigada, A., Manzoni, S., and Mancosu, F. (2006). Measurement of contact forces and patch features by means of accelerometers fixed inside the tire to improve future car active control. Vehicle System Dynamics, vol. 44 (sup1):pp. 3–13.

Brusarosco, M., Cigada, A., Manzoni, S., Brusarosco, M., Cigada, A., and Experimental, S. M. (2008). Experimental investigation of tyre dynamics by means of MEMS accelerometers fixed on the liner Experimental investigation of tyre dynamics by means of MEMS accelerometers fixed on the liner. Vehicle System Dynamics, 46(11):pp. 1013–1028.

Cao, S., Pyatt, S., Anthony, C., Kubba, A., Kubba, A., and Olatunbosun, O. (2016). Flexible Bond Wire Capacitive Strain Sensor for Vehicle Tyres. Sensors, 16(929).

Castillo, J., Blanca, A. P. D. L., Cabrera, J. A., Simón, A., Blanca, A. P. D. L., Cabrera, J. A., and Simón, A. (2006). An optical tire contact pressure test bench. Vehicle System Dynamics, 44(3):pp. 207–221.

Erdogan, G., Alexander, L., and Rajamani, R. (2011). Estimation of Tire-Road Friction Coefficient Using a Novel Wireless Piezoelectric Tire Sensor. IEEE Sensors, 11(2):267–279.

Feldesi, F., Botha, T. R., and Els, P. S. (2019). Three-Dimensional Contact Patch Strain Measurement Inside Rolling Off-Road Tyres. University of Pretoria.

Feldesi, F., Botha, T. R., and Els, P. S. (2020). Full-field strain measurements of the inside of an agricultural tyre using digital image correlation. Journal of Terramechanics, 91:309–318.

Garcia-Pozuelo, D., Olatunbosun, O., Strano, S., and Terzo, M. (2019). A real-time physical model for strain-based intelligent tires. Sensors and Actuators A, 288:1–9.

Garcia-Pozuelo, D., Olatunbosun, O., Yunta, J., and Yang, X. (2017a). A Novel Strain-Based Method to Estimate Tire Conditions Using Fuzzy Logic for Intelligent Tires. Sensors, 17(350):1–16.

Garcia-Pozuelo, D., Yunta, J., Olatunbosun, O., Yang, X., and Diaz, V. (2017b). A Strain-Based Method to Estimate Slip Angle and Tire Working Conditions for Intelligent Tires Using Fuzzy Logic. Sensors, 17(874).

Green, R. W. (2011). A Non-contact Method for Sensing Tire Contact Patch Deformation Using a Monocular Vision System and Speckled Image Tracking. Auburn University.

Guthrie, A. G., Botha, T. R., and Els, P. S. (2017). ScienceDirect 3D contact patch measurement inside rolling tyres. Journal of Terramechanics, 69:13–21.

Guthrie, G., Botha, T., and Els, S. (2015). 3D Computer Vision Inside Off-Road Vehicle Tyres. Proceedings of the 13th ISTVS European Conference.

Hiraoka, N., Matsuzaki, R., and Todoroki, A. (2009). Concurrent Monitoring of In-plane Strain and Out-of-plane Displacement of Tire Using Digital Image Correlation Method. Journal of Solid Mechanics and Materials Engineering, 3(11):1351–1357.

Ivanov, V. (2010). Analysis of Tire Contact Parameters Using Visual Processing. Advances in Tribology, pages 1–11.

Jun, H., Way, T. R., Bailey, A. C., Burt, E. C., and McDonald, T. P. (2004). Dynamic load and inflation pressure effects on contact pressures of a forestry forwarder tire. Journal of Terramechanics, 41:209–222.

Kim, S. J., Kim, K. S., and Yoon, Y. S. (2015). Development of a tire model based on an analysis of tire strain obtained by an intelligent tire system. International Journal of Automotive Technology, 16(5):865–875.

Lee, J., Oh, J., Kim, H., and Choi, B. (2015). Strain-based piezoelectric energy harvesting for wireless sensor systems in a tire. Journal of Intelligent Material Systems and Structures, 26(11):1404–1416.

Matilainen, M. and Tuononen, A. (2015). Tyre contact length on dry and wet road surfaces measured by three-axial accelerometer. Mechanical Systems and Signal Processing, 52-53:548–558.

Matsuzaki, R. and Todoroki, A. (2007). Wireless flexible capacitive sensor based on ultra-flexible epoxy resin for strain measurement of automobile tires. Sensors and Actuators A, 140:32–42.

Matsuzaki, R., Todoroki, A., and Kobayashi, H. (2005). Passive wireless strain monitoring of a tire using capacitance and electromagnetic induction change. Advanced Composite Materials, 14(2):147–164.

Morinaga, H., Wakao, Y., Hanatsuka, Y., and Kobayakawa, A. (2006). The possibility of intelligent tire (technology of contact area information sensing). FISITA World Automotive Congress, pages 1–11.

Muller, S., Uchanski, M., and Hedrick, K. (2003). Estimation of the Maximum Tire-Road Friction Coefficient. Journal of Dynamic Systems, Measurement, and Control, 125:607–617.

Niskanen, A. J. and Tuononen, A. J. (2014). Three 3-axis accelerometers fixed inside the tyre for studying contact patch deformations in wet conditions. Vehicle System Dynamics, 52(sup1):287–298.

Pohl, A., Steindl, R., and Reindl, L. (1999). The " Intelligent Tire " Utilizing Passive SAW Sensors — Measurement of Tire Friction. IEEE Transactions on Instrumentation and Measurement, 48(6):1041–1046.

Raper, R., Bailey, A., Burt, E., Way, T., and Liberati, P. (1995). The effects of reduced inflation pressure on soil-tire interface stresses and soil strength. Journal of Terramechanics, 32(1):43–51.

Tuononen, A. J. (2008). Optical position detection to measure tyre carcass deflections. Vehicle System Dynamics, 46(6):471–481.

Tuononen, A. J. (2011). Laser triangulation to measure the carcass deflections of a rolling tyre. Measurement Science and Technology, 22.

Yang, X. (2011). Finite element analysis and experimental investigation of tyre characteristics for developing strain-based intelligent tyre system. University of Birmingham.

Yunta, J., Garcia-pozuelo, D., Diaz, V., and Olatunbosun, O. (2019). Influence of camber angle on tire tread behavior by an on-board strain-based system for intelligent tires. Measurement, 145:631–639.